A PHYSICS BASED MODEL WITH AN ANKLE/HIP CONTROLLER FOR PREDICTING MOTION INDUCED INTERRUPTIONS

by

James Nickerson

Submitted in partial fulfillment of the
requirements for the degree of
Master of Computer Science

at

Dalhousie University
Halifax, Nova Scotia
June 2014

Table of Contents

List of Tables

List of Figures

Abstract

Ship motions can greatly impact a person's ability to perform their duties at sea. One metric that can be used to measure this is called a Motion Induced Interruption (MII). An MII occurs when a person stops performing their task to readjust their balance or brace themselves against falling. An increase in the number of MIIs encountered will decrease safety and efficiency of a ship and its crew.

Several physics based models have been proposed to predict MIIs at sea, the simplest of which represents the human body as a rigid block with the mass and inertial properties of a typical human. When the ship dynamics are sufficient to cause the block to tip over or slide then an MII is encountered. Another popular approach for MIIs is to use a 2D inverted pendulum model in the sagittal plane. For MIIs in the frontal plane, a four-bar linkage system has been used.

This thesis presents a more sophisticated physics based model that can predict MIIs in both the sagittal and frontal planes. It uses a Reaction Mass Pendulum (RMP) model derived from an inverted pendulum. This model differs from an Inverted Pendulum (IP) model in that the mass is not represented as a single point mass. Instead it distributes the mass into six equal parts, with two point masses along each of the three principal axes. This creates an ellipsoidal representation of the upper body which can be rotated on a spherical joint. The shape of the ellipsoid can be changed to better represent the sailor's pose. A universal joint is used to model the ankle. The RMP model is controlled using an ankle/hip strategy.

To validate the MIIs predicted by the RMP model, motion capture data from a recent sea trial was used. The trial data provided the actual MII times for eight sailors. The ship motions from the trial were fed into two models: an RMP model and a two degree-of-freedom IP model. The predictions from these two models were also compared to a similar sea trial from 2009 where a planar IP model was used. It was found that the two degree-of-freedom IP model outperformed the planar IP model and the RMP model outperformed both IP models.

Acknowledgements

I would like to thank my supervisor, Dirk Arnold, for his guidance and patients throughout the process of this thesis. I would not have been able to complete this work without his support.

Secondly, I would like to thank DRDC for their financial support. I would especially like to thank my group leaders, Jim Colwell and Kevin McTaggart and my section head, Neil Pegg, for providing me with the time to complete this thesis. I would also like to thank Dave Heath for the use of his LabView software and Doug Perrault for his insightful answers to my many questions.

Finally, I would like to thank my wife, Elizabeth, and my sons, Cameron, and Andrew, for their encouragement and love throughout this long process.

Chapter 1

Introduction

Simulating shipboard activities has long been of interest to naval researchers. It is important to understand how a ship reacts in an ocean environment and how those motions affect various operations such as refueling at sea (Figure 1.1), launch and recovery of small crafts (Figure 1.2), or weapons loading (Figure 1.3) to name but a few. Simulations of these operations are useful when designing new ships, developing new tactics, understanding operational limits, or validating experimental data. They can help researchers to find cost saving measures, understand inefficiencies in processes, and develop safer tactics.

Figure 1.1: Refueling at Sea - source: Department of National Defence (photo by Corporal Johanie Maheu)

One aspect that shipboard simulation is often lacking is human factors. In order to carry out these seakeeping activities a person must perform some actions in the presence of external forces caused by the ship's motions, which are sometimes erratic

Figure 1.2: Launching Zodiac from HMCS Toronto - source: Department of National Defence (photo uncredited)

Figure 1.3: Loading Torpedo - source: Department of National Defence (photo by Corporal Shilo Adamson)

in nature. A metric that can be used to measure the ability of a person to perform their duties at sea is called a Motion Induced Interruption (MII). The frequency at which a person has to stop what they are doing in order to adjust their posture or brace themselves from falling because of the ship's motion, will negatively affect their ability to safely and efficiently perform their seakeeping task. The ability to predict when an MII will occur and the conditions that cause the instability is important to help with designing new naval platforms and for developing seakeeping guidance and planning.

Initially, the conventional approach to predicting MIIs modelled the person as a single rigid-body block that had the mass and inertial properties of a typical sailor [17]. An MII would occur when the motions of the ship were enough to cause the block to tip over or to slide on the deck. Although this model greatly simplifies the complexities of human balance, once the model parameters are tuned, it can be a useful tool to examine different seakeeping platforms and the various sea conditions they operate in.

More recently, Langlois et al., have used a single link planar inverted pendulum model [32] and a single link inverted pendulum model with two degrees-of-freedom at the ankle [31] to predict MIIs. One of the disadvantages of using a single link inverted pendulum model is that it represents the entire humanoid body as a point mass, which does not take into account the centroidal moment of inertia. The centroidal moment of inertia directly affects the angular momentum of the body and can be used to maintain postural stability, where linear momentum alone may not suffice.

The RMP, as introduced by Lee and Goswami [33], consists of two components: the "leg" and the "body". The RMP "leg" connects the model's centre of mass to its desired centre of pressure. The "body's" mass is distributed in six equal parts along the three principal axes (two for each axis), and attached to the top of the "leg" using a three degree-of-freedom spherical joint. The positions of the masses along the three axes form an ellipsoid which is used to model the upper trunk of the body as shown in Figure 1.4. The two masses on each axis are modeled with translational joints and are always equal distance from the spherical joint position. The height of the centre of mass is controlled by a translational joint. The ankle is modeled as a universal joint with two degrees-of-freedom. The model has a total of twelve degrees-of-freedom.

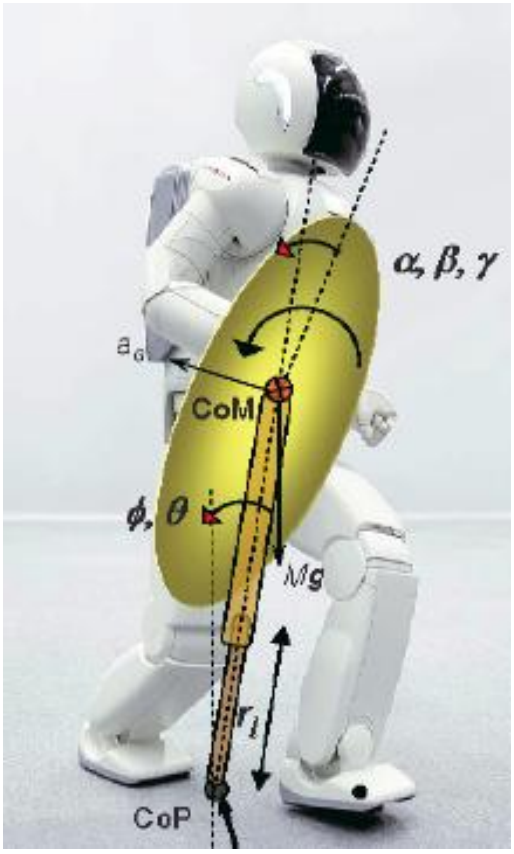

Figure 1.4: Lee and Goswami RMP conceptual diagram (α, β, γ are the rotations of the hip in the x, y, and z axes, ϕ, θ are the 2D rotation angles of the ankle, CoM is the Centre of Mass, CoP is the Centre of Pressure, Mg is the model's mass multiplied by the gravitational acceleration, and r_l is the length of the leg) [33]

The size, shape, and orientation of the ellipsoid can be used to represent the limb movements of the upper body as described by Lee and Goswami [33].

There are two criteria of interest to us when choosing the type of model for predicting MIIs. The first is, it had to be able to compute the dynamic quantities used for predicting MIIs (positions, velocities, and accelerations of the centre of mass and the centre of pressure) in real-time. This would allow it to be incorporated into the existing ship simulation environment of Defence Research and Development Canada (DRDC) - Atlantic. The second criterion is, the model had to have sufficient articulation so that its motions could be mapped to a fully articulated humanoid model to produce reasonable movements. The RMP model is used because it meets the above criteria and it is an extension of the inverted pendulum used successfully by Langlois et al. [32] [31] to predict MIIs. The RMP model was introduced by Lee and Goswami [33] in 2007, and we modified their equations of motion to account for a ground plane that is moving with six degrees-of-freedom.

This thesis employs a 3D Reaction Mass Pendulum (RMP) model for predicting MIIs. The upper body is represented as a rotating ellipsoid which can generate angular momentum at the hip if an ankle strategy alone is not sufficient to keep the model upright. An ankle/hip controller is employed to compute the joint torques and forces required to maintain postural stability. The controller used is based on an ankle/hip controller introduced by Kiemel [28]. It was modified to work with an RMP model attached to a platform moving with six degrees-of-freedom. The model is validated using motion capture data from a 2012 sea trial. The MII predictions from the 2012 sea trial compare quite favorably with the results from a sea trial conducted in 2009 [32] where similar sea conditions existed. In the 2009 trial, a single link, planar, inverted pendulum was used to predict MIIs with 41% accuracy. The RMP model has 66% accuracy for its trial data.

The contributions of this thesis include:

- Updating the equations of motion for Lee and Goswami's RMP model to account for a ground plane that is moving with six degrees-of-freedom.

- Updating Kiemel's ankle/hip controller to work in both the sagittal and frontal planes for an RMP model.

- Predicting MIIs using an RMP model and validating the predictions with observed MII data from a sea trial.

Chapter 2 presents background on modeling human postural stability and predicting MIIs. Chapter 3 derives the equations of motion that were used for the model. The ankle/hip controller is detailed in Chapter 4. The methods used to validate the model are presented in Chapter 5 with a discussion of the results. Chapter 6 gives the conclusions of the research and talks about future areas of research.

Chapter 2

Background

2.1 Introduction

Postural stability at sea is a concern for all types of seakeeping tasks a person is required to perform, from simple activities such as standing to more dynamic actions like walking, running, or moving heavy loads. Naval researchers have developed many types of models over the years for analyzing postural stability in moving environments. The humanoid models range in complexity from the very simple single rigid body with no articulation [17] to more complex, multi-body articulated models [26].

Initial research was done with the goal of understanding how humans maintain balance in the presence of motions but more recently the models have been used to help quantify and measure the performance of shipboard activities.

This chapter will give an overview of the research into postural stability and motion induced interruptions that have been carried out over the past 40+ years. It looks at physiological aspects of human balance control, the physics of postural stability, and the techniques used to validate the research carried out.

2.2 The Physiology of Balance

Even for simple activities like quiet standing, the human body requires many minor corrections in muscle control and joint movements to maintain its balance. This is a result of the inherent instability caused by the height of a person's centre of mass and the highly actuated nature of a person's body [3].

There are three main systems the human body uses to keep itself upright: the vision system, the proprioceptive system, and the vestibular system [41].

The Vision System: This system is part of the central nervous system. It is used to process visual information and helps a person to interpret their surroundings and assess the distance to and between objects.

The Proprioceptive System: This system provides information on what the body's muscles and joints are doing. It informs us of how and when our muscles are stretching and contracting and how joints are being activated. It enables an awareness of how our bodies are moving in space.

The Vestibular System: This is the sensory system which is responsible for responding to accelerated and decelerated movements. It helps the body understand its position in space. It has interconnections with many parts of the body and helps form a basis for all sensory inputs.

The degree to which each of these three systems reacts to motion disturbances is different. Because of this, postural stability maintenance varies relative to motion characteristics such as frequency and amplitude, and to the availability of sensory information.

To model this type of sensory system, feedback control is typically used. The sensory information is interpreted as kinematic data that is fed into a control system. The control system then calculates torques and forces and applies them to the model's joints and segments. The applied forces cause the dynamic model to react and these reactions are fed back into the control system to start the next cycle of the feedback loop, as shown in Figure 2.1.

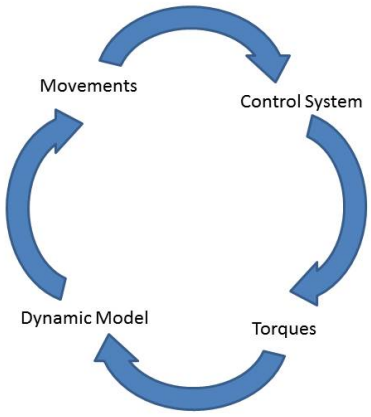

Figure 2.1: Postural Stability Feedback Model

Some researchers have postulated that balance control consists of both feedback and feedforward components. They theorize that the body incorporates a database of finely tuned, predetermined reflexive postural responses. It has been hypothesized [4, 54] that the body does not engage in postural control unless the disturbances exceed a certain threshold. This can simplify the task of stability control when the environment is relatively stable and compensates for the time delay related to data transmission and feedback control for decision processes.

2.3 Humanoid Balance Models

Human balance control models are defined by the dynamics of postural stability [18]. Many dynamic models have been used to simulate both walking gaits and quiet standing. The models developed over the past four decades can be broadly grouped into one of three categories:

Sagittal Plane Only: These models use a planar inverted pendulum with one to five links to measure motions in the sagittal plane (See Figure 2.2).

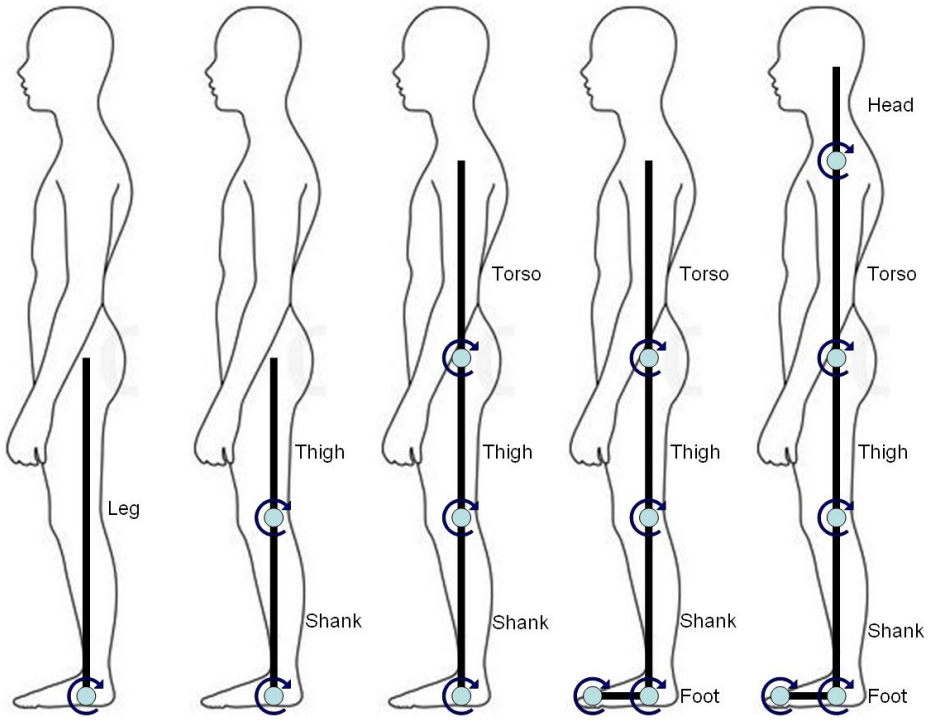

Figure 2.2: One, Two, Three, Four, and Five-Link Planar Inverted Pendulum Models

Frontal Plane Only: These models use a four-bar linkage system to measure motions in the frontal plane (See Figure 2.3).

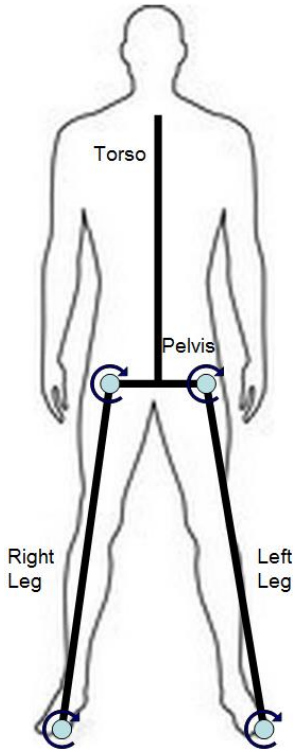

Figure 2.3: Four-Bar Linkage Model

Sagittal and Frontal Plane: These models use an inverted pendulum with two degrees-of-freedom at the ankle to measure motions in the sagittal and frontal planes (See Figure 2.4).

2.3.1 Sagittal Plane Models

The single-link inverted pendulum model has been used by Gubina et al. [18] in 1974, Hemami [20] in 1977, Hemami et al. [23] in 1982, Peeters et al. [44] in 1985, Patton et al. [42] [43] in 1997 and 1999, and Langlois [32] [30] in 2009 and 2010. A single 1D rotational joint is used to represent an ankle.

Two-link planar inverted pendulum models have been used by Hemami and Goliday [22] in 1976, Hemami and Jaswa [24] in 1978, and Wu [55] in 2000. Two rotational joints are used where each has a single degree-of-freedom. One is used to represent the ankle and the other is used to represent the knee.

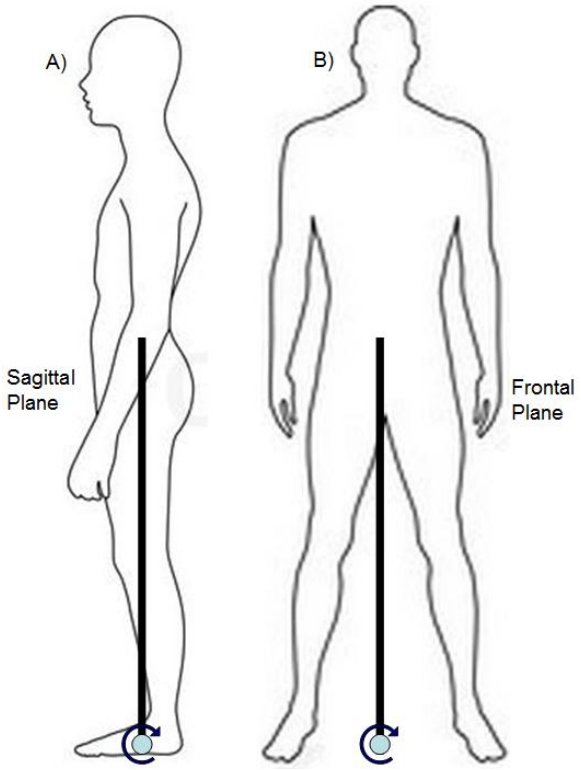

Figure 2.4: Two Degree-Of-Freedom Inverted Pendulum Model - View A shows the motions in the Sagittal plane and view B shows the motions in the frontal plane.

Three-link planar inverted pendulum models have been used by Chow and Jacobson [5] in 1972, Hemami and Jaswa [24] in 1978, Hemami et al. [21] in 2006, and Humphrey et al. [26] in 2010. Three, 1D rotational joints are used to model the ankle, knee and hip.

In 1980, Koozekanani et al. [29] used a four-link planar inverted pendulum model and in 1981, Stockwell et al. [51] extended Koozekanani's model by adding a fifth link to model the motions of the head. Five single dimensional, rotational joints are used to model the toe, the ankle, the knee, the hip, and the head motions.

2.3.2 Frontal Plane Models

Frontal plane models have been used by Iqbal et al. [27] in 1993, Scrivens et al. [50] in 2006, and Langlois [30] in 2010. The four-bar model uses four rotational joints which each have one degree of freedom to measure side-to-side swaying motions in quiet standing.

2.3.3 Sagittal and Frontal Plane Models

A single link inverted pendulum model with a two degree-of-freedom joint at the 'ankle' has been used by Wu et al. [56] in 1998 and Langlois et al. [31] in 2013. The ankle is modeled as a 2D universal joint as seen in Figure 2.4.

2.4 Humanoid Balance Controllers

Many of the models from the previous section use a two-dimensional inverted pendulum with a varying number of links to describe human postural stability. Nashner's PhD thesis [40] from 1970 was the catalyst for many of the controllers developed over the past four decades. His thesis discussed how to control postural stability using different types of sensory feedback and the paths they take through the body. Nashner said there should be a difference between quiet standing where no external perturbations exist and situations where external forces are acting on the model.

There are two approaches to modeling quiet standing under small perturbations that are generally used [31]. The first approach involves measuring the position of the centre of mass and centre of pressure and applying a control scheme based on

how those quantities are changing. The second approach involves measuring the joint positions and velocities and developing a control scheme based on how those quantities change. The former method is often used to analyze experimental data where it is easier and more cost effective to capture the centre of mass and pressure than it is to capture the position of the joints. The latter method is usually used for developing control strategies based on mathematical models since it allows for full feedback control.

2.5 Motion Induced Interruption (MII) Models and Experiments

Physiological-inspired models have been used to better understand human postural stability. They also present the potential for measuring the effects of external motions on human performance. The need for this understanding is highlighted in ship activities where crew members are required to perform a wide variety of seakeeping tasks in a motion environment. The ability of sailors to walk, lift, or move heavy objects on the deck [37] can be impaired by a ship's motion, causing increased injuries, decreased efficiency, or increased costs. In 1984, Baitis and Applebee [1] defined a means to measure the amount of reduced productivity based on the number of times a person adjusts their stance to maintain balance. Motion Induced Interruptions (MIIs) were defined in 1990 to be incidents where a person would take a step, grab hold, or stop what they are doing to maintain their stability [16]. Measuring MIIs requires knowledge of the environment and how it is influencing the subjects. By quantifying postural stability in moving environments, useful data can be obtained that provides operational and/or design guidance.

Traditional bio-mechanical models were not designed to measure MIIs but more recently there have been several models implemented to investigate these events.

The earliest MII model developed was the Graham model in the early 90's [17]. It used a single rigid block with mass and inertial properties of an average person. An MII would occur if the ship's motion was sufficient to cause the block to tip over or slide on the deck. Thresholds were defined based on the properties of the block such as the centre of mass or the coefficient of friction at the base. An unoccupied chair was observed to validate sliding MIIs by comparing its actual sliding events with those predicted by the model. A tipping event occurs when the moment about

the block falls to zero as seen in Figure 2.5.

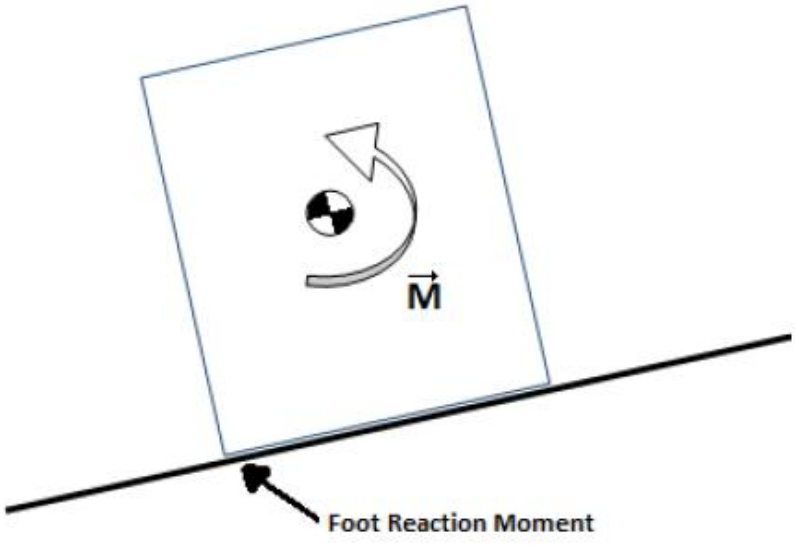

Figure 2.5: Moments in the Graham et al. MII Model. [17]

A large motion simulator located at the Defense Research Agency in the United Kingdom was used to conduct a series of experiments from 1996 through 1998 [7, 8, 10]. The motion platform was able to produce acceleration in five degrees of freedom. Subjects were required to perform a variety of seakeeping tasks. The data from these experiments was used to develop thresholds for the Graham model for predicting tipping and sliding events. The tuned model provided good MII predictions though it tended to under-predict when the MII rate was high. The experimental data was also used to investigate a statistical model from MII prediction.

In 1993, McIlroy and Maki [38] examined the psychological effects that contribute to MIIs. They either allowed a subject to react to external forces by taking a step or instructed them to try and not react to the force. The results showed when a person was permitted to step the occurrence of stepping motions increased compared to the group that was instructed not to step. This indicated that MIIs were caused by more than the dynamics occurring at the time of the event. Maki and McIlroy [35] continued their research in 1997 by investigating fixed stance versus non-fixed stance recovery methods. For fixed stance a person could bend at the hips, knees, or ankles to maintain stability. For non-fixed stance they could take a step or grab a support hold. The results showed a person will step long before they are required to do so

when using non-fixed stance recovery methods.

In 2004, McKee [39] used a two plane articulated model to investigate MII prediction. An inverted pendulum model was used for motions in the sagittal plane and a four-bar linkage model was used in the frontal plane as shown in Figure 2.6.

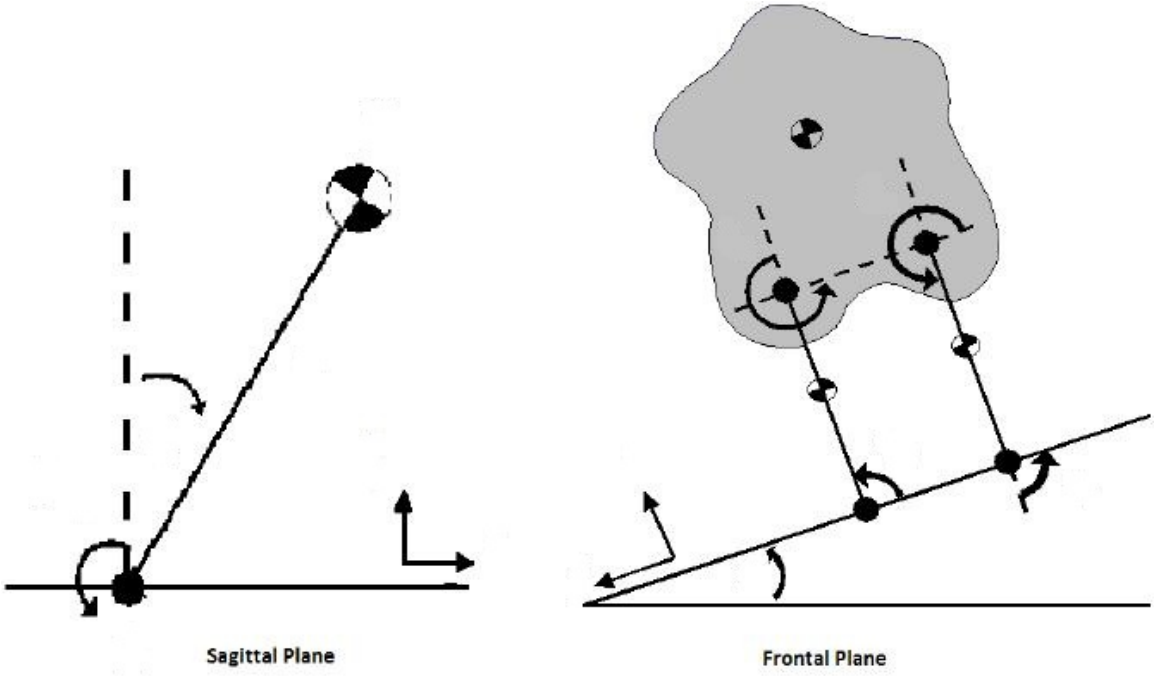

Figure 2.6: McKee frontal and sagittal plane models. [39]

A controller was used for the ankle joint which was tuned using data recorded at the Naval Biodynamics Laboratory [2]. McKee's model slightly under predicted the number of MIIs while the Graham model over predicted the number of MIIs. McKee suggested an articulated model was a viable alternative to the Graham model.

Duncan et al. [12, 11] performed a series of experiments in 2007 and 2009 to investigate MIIs. In 2009, eleven participants were used to determine the effect of thoracolumbar kinematics and foot centre of pressure on balance. The subjects performed two different tasks at different sea states. The first task consisted of stationary standing with feet shoulder width apart and arms by their side. The second task was holding a 10kg weight in a dead-lift with arms straight and the load held against their thighs. Data was collected on the thoracolumbar kinematics, velocity of the centre of pressure, and video capture of the MII events. From examining the MIIs it was discovered that sudden postural changes resulted in significant increases to the

average and peak thoracolumbar velocities. This confirmed that the number of MIIs was influenced by the direction the subject was standing and that both body and foot movements were required to maintain postural stability.

In 2008, Hasson et al. [19] performed postural stability experiments where they attached a participant to a flat board so motions in the sagittal plane were minimized as shown in Figure 2.7. The subjects could only maintain balance using their ankles. A variable force was applied from behind and the subject's ability to not take a step was recorded. The results were compared to a pendulum model developed by Hof et al [25]. Approximation curves for the centre of mass acceleration versus the applied force were derived from the data.

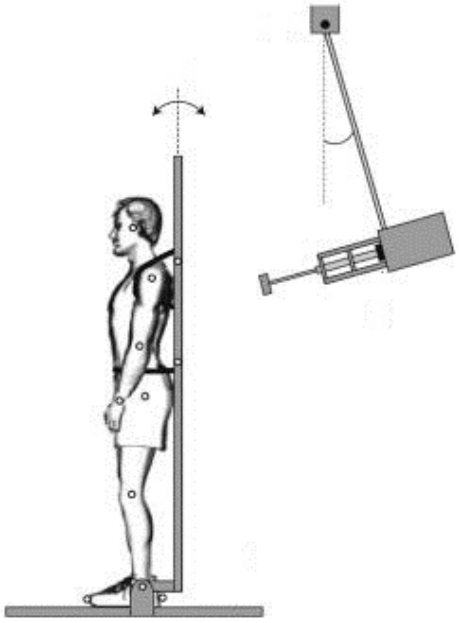

Figure 2.7: Hasson et al. experimental setup. [19]

In 2010, Langlois [30] presented a three-dimensional inverted pendulum model for predicting MIIs. The translational and rotational components of the model were derived separately. The rotational components were solved using Newton-Euler equations to determine the ankle yaw. The translational components are solved to get the forces at the base of the pendulum. A controller was used to stabilize the pendulum using ankle moments. The controller is tuned to maintain an upright stance using applicable dampening. The model is used to predict both tipping and sliding events. It was validated using available sea trial data and data from a motion platform. The

inverted pendulum contained one segment and had two revolute degrees of freedom at the ankle.

Stoffregen et al. [52] performed experiments on experienced sailors in 2011 on land and at sea. They investigated the influence of ship motion on postural balance by varying the participants' stance width while performing visual tasks. The visual performance was similar for both land and sea. Postural stability was influenced by the stance width and the difficulty of the visual task being performed. They also noted that postural stability was influenced by the number of days at sea. For the bodys anterior-posterior axis (which corresponded to the motion of the ship along its sway axis), postural activity was highest for the first day and then leveled out for the remaining days. For the bodys mediolateral axis (which corresponded to the motion of the ship along its surge axis), changes in postural activity exhibited a U-shaped function, with a minimum on the third day. Their findings confirmed the hypothesis that task performance is affected, in part, by postural activities.

Matsangus and McCauley [36] conducted experiments in 2013 using a six degree of freedom motion platform. They investigated the relationship between sway parameters and MIIs in a controlled environment as well as the effects of acceleration frequency on MII occurrences. Only tipping events in the sagittal plane were considered. Their research confirmed that the occurrence of MIIs increased as peak sway increased. They also noted that tipping was more likely for complex multidirectional motions than for unidirectional motions. A new term called "probable" MII was introduced to refer to a temporary loss of balance that did not result in a tipping event. The data from their research was used to implement a mathematical model for predicting MII occurrences.

Also in 2013, Langlois et al. [31] developed a mechanical, single link, inverted pendulum model with a two degree-of-freedom universal joint at the ankle as seen in Figure 2.8. The mechanical model was used on a motion platform to detect MIIs and provided data for tuning and validating a mathematical model of the system.

2.6 Conclusion

While many inverted pendulum postural stability models have been developed for more than four decades, few have been derived in three dimensions. Langlois' work

Figure 2.8: Langlois et al. spatial inverted pendulum model. [31]

[32] [31] on using articulated models to predict MIIs has shown that this is a viable direction for new research. A limitation of Langlois's work is that his single link inverted pendulum model is incapable of generating angular momentum to help with postural stability. The RMP model presented in this thesis can generate both linear and angular momentum.

Chapter 3

Reaction Mass Pendulum Model

3.1 Introduction

The RMP, as introduced by Lee and Goswami [33], is a hierarchical model consisting of 9 massless links, 6 point masses, 1 universal joint, 1 spherical joint, and 7 prismatic joints as shown in Figure 3.1. The ground plane is the base of the structure and the links are attached to one-another by joints such that no loops exist in the system. The pairs of point masses along each principal axis are constrained such that their distance from the spherical joint is always the same.

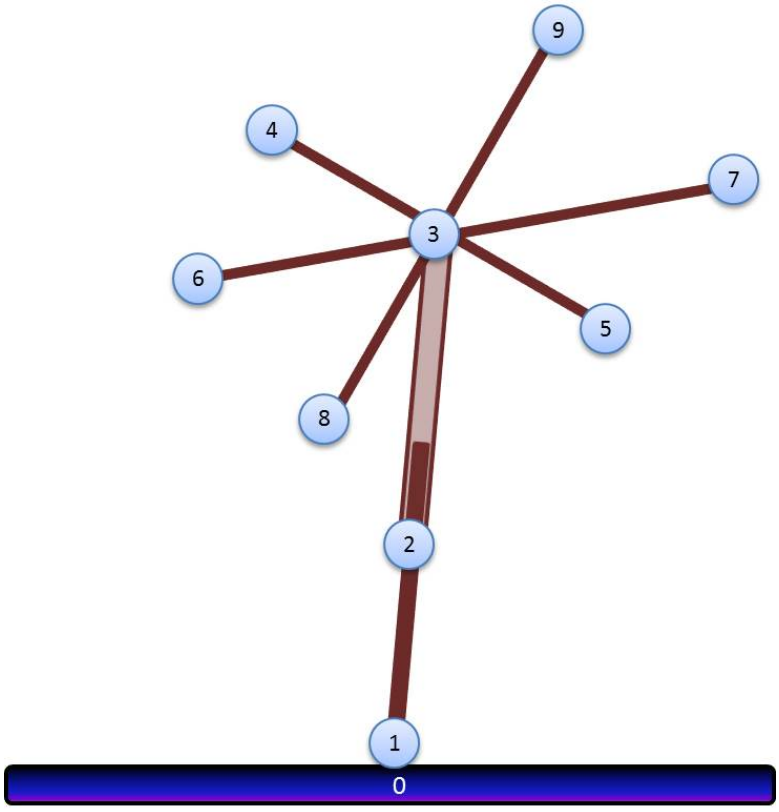

Figure 3.1: RMP Hierarchical View (0 - Ground Plane, 1 - Universal Joint, 2 - Translational Joint, 3, Spherical Joint, 4 through 9 - Translational Joints. The 6 point masses are attached to joints 4-9.)

Spatial notation is used to reduce the number of equations when deriving the equations-of-motion for the RMP model. It combines the linear and angular components into a single equation as discussed in Section 3.2. The joints are modeled as kinematic connections between rigid bodies as described in Section 3.3.

The equations of motion are derived using a forward dynamic solution for chained structures. The equations of motion of the RMP model are found in Section 3.4.

3.2 Spatial Notation

Roy Featherstone [13] coined the term "spatial notation" to refer to a six-dimensional vector quantity that encapsulates both rotational and translational motion. This concise notation can be used to describe dynamic properties such as velocities, accelerations, and forces. In this document,

$$\mathrm{v} = \begin{bmatrix} \boldsymbol{\omega} \\ \boldsymbol{v} \end{bmatrix}$$

represents a spatial velocity with the three-dimensional angular component $\boldsymbol{\omega}$ and three-dimensional linear component $\boldsymbol{v}$. As well,

$$\mathrm{a} = \begin{bmatrix} \dot{\boldsymbol{\omega}} \\ \dot{\boldsymbol{v}} \end{bmatrix}$$

represents a spatial acceleration with the angular acceleration component $\dot{\boldsymbol{\omega}}$ and linear acceleration component $\dot{\boldsymbol{v}}$. The torques and linear forces are combined into a spatial force vector as follows,

$$\mathrm{f} = \begin{bmatrix} \boldsymbol{\tau} \\ \mathbf{f} \end{bmatrix}$$

A 6×6 matrix, I, is used to represent the spatial inertia matrix of a rigid body,

$$\mathrm{I} = \begin{bmatrix} \mathbf{I}_{3\times3} & m\widetilde{\mathbf{d}} \\ m\widetilde{\mathbf{d}}^T & m\mathbf{1}_{3\times3} \end{bmatrix}$$

where $\mathbf{I}_{3\times3}$ is a 3×3 moment of inertia matrix with respect to the origin of the coordinate system, m is the mass of the body, $\mathbf{1}_{3\times3}$ is a 3×3 identity matrix, and $\widetilde{\mathbf{d}}$

is the position of the centre of mass for the body written as a 3×3 matrix as shown in Appendix A.

A 6×6 transformation matrix will transform a spatial vector quantity from one coordinate frame to another. The following 6×6 transformation matrix ($\mathrm{X}_{\alpha,\beta}$) will transform a spatial vector from coordinate frame α to coordinate frame β:

$$\mathrm{X}_{\alpha,\beta} = \begin{bmatrix} \mathbf{A} & \mathbf{0}_{3\times3} \\ \mathbf{0}_{3\times3} & \mathbf{A} \end{bmatrix} \begin{bmatrix} \mathbf{I}_{3\times3} & \mathbf{0}_{3\times3} \\ \widetilde{\mathbf{b}}^T & \mathbf{I}_{3\times3} \end{bmatrix} = \begin{bmatrix} \mathbf{A} & \mathbf{0}_{3\times3} \\ \mathbf{A}\widetilde{\mathbf{b}}^T & \mathbf{A} \end{bmatrix}$$

where $\mathbf{A}$ is the 3×3 rotation matrix which aligns the α-coordinate system to the β-coordinate system, $\widetilde{\mathbf{b}}$ is the origin of the β-coordinate system expressed in α-coordinates, $\mathbf{I}_{3\times3}$ is a 3×3 identity matrix, and $\mathbf{0}_{3\times3}$ is a 3×3 null matrix.

3.3 Modeling the Joints

Joints can be defined mathematically as the kinematic interconnection between two rigid bodies. The two bodies can have anywhere from zero to six degrees-of-freedom (three rotational and three translational) with respect to each other. Three types of joints were used in constructing the RMP model. The notation used in the equations-of-motion has been taken from Roberson and Schwertassek [49]:

Prismatic Joint: A joint containing one translational degree-of-freedom.

Universal Joint: A joint containing two rotational degrees of freedom.

Spherical Joint: A joint containing three rotational degrees of freedom.

A joint's movement can be described by two sparse matrices which define the free modes (allowable degrees-of-freedom), called $\boldsymbol{\phi}$ and the constrained modes (locked degrees-of-freedom), called $\overline{\boldsymbol{\phi}}$. Together, these two matrices form a 6×6 matrix that defines the axes on which the joint can rotate and/or translate. The following relationship exists between the $\boldsymbol{\phi}$ and $\overline{\boldsymbol{\phi}}$ matrices,

$$\begin{bmatrix} \boldsymbol{\phi}^T \\ \overline{\boldsymbol{\phi}}^T \end{bmatrix} \begin{bmatrix} \boldsymbol{\phi} & \overline{\boldsymbol{\phi}} \end{bmatrix} = \begin{bmatrix} \mathbf{I}_{N\times N} & \mathbf{0}_{N\times(6-N)} \\ \mathbf{0}_{(6-N)\times N} & \mathbf{I}_{(6-N)\times(6-N)} \end{bmatrix}$$

where N is the number of degrees-of-freedom for the joint. A joint's relative velocity can be described by the equation,

$$\mathbf{v} = \boldsymbol{\phi}\dot{\mathbf{q}}$$

where $\dot{\mathbf{q}}$ contains a velocity variable for each of the N degrees-of-freedom for the joint.

3.3.1 Prismatic Joint

Seven prismatic joints are used in the RMP model. One is used to adjust the height of the centre of mass and the other six are used to move the six masses along the principal axes (+x/-x, +y/-y, +z/-z). The masses along the principal axes are constrained such that each mass is at an equal distance from the spherical joint. Each joint has a single translational degree-of-freedom. The state of the joint can be represented by its position along the axis and the velocity at which it travels. For example a prismatic joint along the y axis can be represented as follows:

state variables: $q = y, \dot{q} = \dot{y}$

positional constraint equations: $\mathbf{b}(q) = \begin{bmatrix} 0 \\ y \\ 0 \end{bmatrix}, \mathbf{A}(q) = \mathbf{1}_{3\times 3}$ (i.e. no rotation)

mode vectors: $\boldsymbol{\phi} = \begin{bmatrix} 0 \\ 0 \\ 0 \\ 0 \\ 1 \\ 0 \end{bmatrix}, \overline{\boldsymbol{\phi}} = \begin{bmatrix} 1 & 0 & 0 & 0 & 0 \\ 0 & 1 & 0 & 0 & 0 \\ 0 & 0 & 1 & 0 & 0 \\ 0 & 0 & 0 & 1 & 0 \\ 0 & 0 & 0 & 0 & 0 \\ 0 & 0 & 0 & 0 & 1 \end{bmatrix}$

kinematic equation of motion: $\frac{\mathbf{dq}}{\mathbf{dt}} = \dot{\mathbf{q}}$

3.3.2 Universal Joint

A universal joint is used to model the "ankle" with two rotational degrees-of-freedom. This joint differs from the previous joint in that its free mode vector has components that depend on the joint's current orientation. The position of the universal joint is represented by two rotations, θ_x and θ_z. The velocity is represented by the variables, $\dot{\theta_x}$ and $\dot{\theta_z}$. The following are used to describe the joint's state:

state variables: $\mathbf{q} = (\theta_x, \theta_z), \dot{q} = (\dot{\theta_x}, \dot{\theta_z})$

positional constraint equations: $\mathbf{b}(\mathbf{q}) = \mathbf{0}_{3\times1}$

$$\mathbf{A}_z = \begin{bmatrix} \cos\theta_z & -\sin\theta_z & 0 \\ \sin\theta_z & \cos\theta_z & 0 \\ 0 & 0 & 1 \end{bmatrix}, \mathbf{A}_x = \begin{bmatrix} 1 & 0 & 0 \\ 0 & \cos\theta_x & -\sin\theta_x \\ 0 & \sin\theta_x & \cos\theta_x \end{bmatrix}$$

$$\mathbf{A}(q) = A_z A_x = \begin{bmatrix} \cos\theta_z & -\sin\theta_z\cos\theta_x & \sin\theta_z\sin\theta_x \\ \sin\theta_z & \cos\theta_z\cos\theta_x & -\cos\theta_z\sin\theta_x \\ 0 & \sin\theta_x & \cos\theta_x \end{bmatrix}$$

mode vectors: $\boldsymbol{\phi} = \begin{bmatrix} 1 & 0 \\ 0 & \cos\theta_x \\ 0 & \sin\theta_x \\ 0 & 0 \\ 0 & 0 \\ 0 & 0 \end{bmatrix}, \overline{\boldsymbol{\phi}} = \begin{bmatrix} 0 & 0 & 0 & 0 \\ -\sin\theta_x & 0 & 0 & 0 \\ \cos\theta_x & 0 & 0 & 0 \\ 0 & 1 & 0 & 0 \\ 0 & 0 & 1 & 0 \\ 0 & 0 & 0 & 1 \end{bmatrix}$

kinematic equation of motion: $\frac{\mathbf{dq}}{\mathbf{dt}} = \begin{bmatrix} \dot{\theta_x} \\ \dot{\theta_z} \end{bmatrix}$

3.3.3 Spherical Joint

A spherical joint is used to orient the six point masses. It has three rotational degrees-of-freedom. To avoid gimbal lock, which occurs when two of the three rotations are driven into a parallel configuration causing the loss of the third degree-of-freedom, a quaternion is used to represent the position of the spherical joint.

A unit quaternion is a vector of four parameters $(s_\varphi, s_x, s_y, s_z)$ that satisfies the normality constraint $s_\varphi^2 + s_x^2 + s_y^2 + s_z^2 = 1.0$ and prescribes a rotation of $2\arccos(s_\varphi)$ radians about the $(s_x, s_y, s_z)^T$ axis.

The joint's relative angular velocity is represented by the vector ω. The following variables are used to represent the state of the prismatic joint:

state variables: $\mathbf{q} = (s_\varphi, s_x, s_y, s_z), \dot{\mathbf{q}} = \boldsymbol{\omega}$

positional constraint equations: $\mathbf{b}(\mathbf{q}) = \mathbf{0}_{3\times1}$, (i.e. no translation)

$$\mathbf{A}(\mathbf{q}) = 2\begin{bmatrix} \frac{1}{2} - s_y^2 - s_z^2 & s_x s_y + s_\varphi s_z & s_x s_z - s_\varphi s_y \\ s_x s_y - s_\varphi s_z & \frac{1}{2} - s_x^2 - s_z^2 & s_y s_z + s_\varphi s_x \\ s_x s_z + s_\varphi s_y & s_y s_z - s_\varphi s_x & \frac{1}{2} - s_x^2 - s_y^2 \end{bmatrix}$$

mode vectors: $\boldsymbol{\phi} = \begin{bmatrix} \mathbf{1}_{3\times3} \\ \mathbf{0}_{3\times3} \end{bmatrix}, \overline{\boldsymbol{\phi}} = \begin{bmatrix} \mathbf{0}_{3\times3} \\ \mathbf{1}_{3\times3} \end{bmatrix}$

kinematic equation of motion: $\frac{\mathbf{dq}}{\mathbf{dt}} = \frac{1}{2} \begin{bmatrix} -s_x & -s_y & -s_z \\ s_\varphi & -s_z & s_y \\ s_z & s_\varphi & -s_x \\ -s_y & s_x & s_\varphi \end{bmatrix} \begin{bmatrix} \omega_x \\ \omega_y \\ \omega_z \end{bmatrix}$

3.4 Equations of Motion

This section describes the equations of motion governing the RMP model's movements (See Figure 3.2) using a recursive Newton-Euler approach. The links that make up the pendulum have a hierarchical structure where each link is connected to a neighbour via a joint. The forces acting on a link are the result of the velocity and accelerations of its parent and child links as well as the relative joint motions and accelerations. Detailed derivations of the Newton-Euler equations can be found in Craig [6] or Featherstone [14].

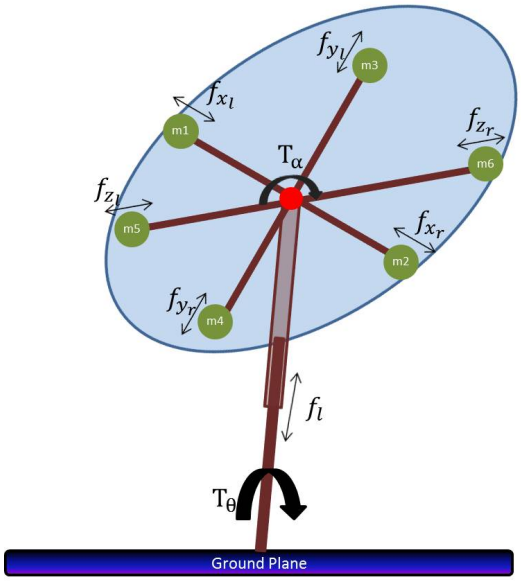

Figure 3.2: RMP conceptual diagram.

The spatial velocity of an arbitrary link i is composed of link i's joint velocity and that of its parent transformed to the current link's inertial frame. The velocity

of link i can be written as:

$$\mathrm{v}_i = \mathrm{X}_i \mathrm{v}_{i+1} + \boldsymbol{\phi}_i \dot{\boldsymbol{q}}_i \tag{3.1}$$

The spatial acceleration of an arbitrary link i is composed of the acceleration of link i's parent (link *i+1*) transformed to the current link's inertial frame, plus the acceleration caused by the rotation of the coordinate frame, and the acceleration of joint i. It can be written as:

$$\mathrm{a}_i = \mathrm{X}_i \mathrm{a}_{i+1} + \zeta_i + \boldsymbol{\phi}_i \ddot{\boldsymbol{q}}_i \tag{3.2}$$

where

$$\zeta_i = \begin{bmatrix} \mathbf{0}_{3\times 1} \\ \mathbf{A}_i(\boldsymbol{\omega}_{i+1} \times (\boldsymbol{\omega}_i \times \mathbf{b}_i)) \end{bmatrix} + \begin{bmatrix} \mathbf{A}_i \tilde{\boldsymbol{\omega}}_{i+1} & \mathbf{0}_{3\times 3} \\ \mathbf{0}_{3\times 3} & 2\mathbf{A}_i \tilde{\boldsymbol{\omega}}_{i+1} \end{bmatrix} \boldsymbol{\phi}_i \dot{\mathbf{q}}_i$$

The laws of Newton and Euler can be combined into a single spatial notation equation which accounts for inertial forces, external forces, and forces propagated from neighbouring links into a single vector. Since quiet standing is being simulated by the RMP model no external, centripetal or coriolis forces are present. This means the Newton-Euler laws can be written as,

$$\mathrm{I}_i \mathrm{a}_i = f_i - \sum_{j | i = parent(j)} \mathrm{X}_j^T f_j \tag{3.3}$$

Using equation (3.3) and solving for the joint forces, the force balance equations for the RMP model can be written as,

$$f_1 = \mathrm{X}_2^T f_2 \tag{3.4}$$

$$f_2 = \mathrm{X}_3^T f_3 \tag{3.5}$$

$$f_3 = (\mathrm{X}_4^T f_4 + \mathrm{X}_5^T f_5 + \mathrm{X}_6^T f_6 + \mathrm{X}_7^T f_7 + \mathrm{X}_8^T f_8 + \mathrm{X}_9^T f_9) \tag{3.6}$$

$$f_4 = \mathrm{I}_4 \mathrm{a}_4 \tag{3.7}$$

$$f_5 = \mathrm{I}_5 \mathrm{a}_5 \tag{3.8}$$

$$f_6 = \mathrm{I}_6 \mathrm{a}_6 \tag{3.9}$$

$$f_7 = \mathrm{I}_7 \mathrm{a}_7 \tag{3.10}$$

$$f_8 = \mathrm{I}_8 \mathrm{a}_8 \tag{3.11}$$

$$f_9 = \mathrm{I}_9 \mathrm{a}_9 \tag{3.12}$$

where f_1 are the spatial forces at the ankle, f_2 are the spatial forces controlling the height of the RMP, f_3 are the spatial forces at the hip controlling the orientation of the ellipsoid, and the remaining spatial forces ($f_4, f_5, f_6, f_7, f_8, f_9$) are controlling the position of the six masses along the three axes (See Figure 3.1).

The forces acting on a body can also be described as the addition of the unconstrained forces and the constrained forces acting on a joint with the following equation,

$$\mathrm{f} = \boldsymbol{\phi}\boldsymbol{\lambda} + \overline{\boldsymbol{\phi}}\,\overline{\boldsymbol{\lambda}} \tag{3.13}$$

where $\boldsymbol{\lambda}$ is the vector of forces in the unconstrained directions and $\overline{\boldsymbol{\lambda}}$ is the vector of forces acting in the constrained directions. Equation (3.13) can be used for each joint of the RMP model. The $\boldsymbol{\lambda}$ values are replaced with the joint's linear or angular force variable to produce the following nine equations,

$$\boldsymbol{\phi}_1\lambda_1 + \overline{\boldsymbol{\phi}_1}\,\overline{\lambda_1} = \mathrm{X}_2^T(\boldsymbol{\phi}_2\lambda_2 + \overline{\boldsymbol{\phi}_2}\,\overline{\lambda_2}) \tag{3.14}$$

$$\boldsymbol{\phi}_2\lambda_2 + \overline{\boldsymbol{\phi}_2}\,\overline{\lambda_2} = \mathrm{X}_3^T(\boldsymbol{\phi}_3\lambda_3 + \overline{\boldsymbol{\phi}_3}\,\overline{\lambda_3}) \tag{3.15}$$

$$\begin{aligned}\boldsymbol{\phi}_3\lambda_3 + \overline{\boldsymbol{\phi}_3}\,\overline{\lambda_3} = {} & \mathrm{X}_4^T(\boldsymbol{\phi}_4\lambda_4 + \overline{\boldsymbol{\phi}_4}\,\overline{\lambda_4}) + \mathrm{X}_5^T(\boldsymbol{\phi}_5\lambda_5 + \overline{\boldsymbol{\phi}_5\lambda_5}) + \\ & \mathrm{X}_6^T(\boldsymbol{\phi}_6\lambda_6 + \overline{\boldsymbol{\phi}_6}\,\overline{\lambda_6}) + \mathrm{X}_7^T(\boldsymbol{\phi}_7\lambda_7 + \overline{\boldsymbol{\phi}_7}\,\overline{\lambda_7}) + \\ & \mathrm{X}_8^T(\boldsymbol{\phi}_8\lambda_8 + \overline{\boldsymbol{\phi}_8}\,\overline{\lambda_8}) + \mathrm{X}_9^T(\boldsymbol{\phi}_9\lambda_9 + \overline{\boldsymbol{\phi}_9}\,\overline{\lambda_9})\end{aligned} \tag{3.16}$$

$$\boldsymbol{\phi}_4\lambda_4 + \overline{\boldsymbol{\phi}_4}\,\overline{\lambda_4} = \mathrm{I}_4\mathrm{a}_4 \tag{3.17}$$

$$\boldsymbol{\phi}_5\lambda_5 + \overline{\boldsymbol{\phi}_5}\,\overline{\lambda_5} = \mathrm{I}_5\mathrm{a}_5 \tag{3.18}$$

$$\boldsymbol{\phi}_6\lambda_6 + \overline{\boldsymbol{\phi}_6}\,\overline{\lambda_6} = \mathrm{I}_6\mathrm{a}_6 \tag{3.19}$$

$$\boldsymbol{\phi}_7\lambda_7 + \overline{\boldsymbol{\phi}_7}\,\overline{\lambda_7} = \mathrm{I}_7\mathrm{a}_7 \tag{3.20}$$

$$\boldsymbol{\phi}_8\lambda_8 + \overline{\boldsymbol{\phi}_8}\,\overline{\lambda_8} = \mathrm{I}_8\mathrm{a}_8 \tag{3.21}$$

$$\boldsymbol{\phi}_9\lambda_9 + \overline{\boldsymbol{\phi}_9}\,\overline{\lambda_9} = \mathrm{I}_9\mathrm{a}_9 \tag{3.22}$$

The above equations can be solved for the unconstrained forces by multiplying both sides of the equations by $\boldsymbol{\phi}^T$ and can be solved for the constrained forces by multiplying both sides of the equation by $\overline{\boldsymbol{\phi}^T}$. This produces the eighteen equations found below (Note: $\mathrm{I}_4 = \mathrm{I}_5 \ldots = \mathrm{I}_9$ and $\boldsymbol{\phi}_4^T = \boldsymbol{\phi}_5^T$, $\boldsymbol{\phi}_6^T = \boldsymbol{\phi}_7^T$, $\boldsymbol{\phi}_8^T = \boldsymbol{\phi}_9^T$),

$$\lambda_1 = \boldsymbol{\phi}_1^T \mathrm{X}_2^T (\boldsymbol{\phi}_2 \lambda_2 + \overline{\boldsymbol{\phi}_2}\,\overline{\lambda_2}) \tag{3.23}$$

$$\overline{\lambda_1} = \overline{\boldsymbol{\phi}_1^T} \mathrm{X}_2^T (\boldsymbol{\phi}_2 \lambda_2 + \overline{\boldsymbol{\phi}_2}\,\overline{\lambda_2}) \tag{3.24}$$

$$\lambda_2 = \boldsymbol{\phi}_2^T \mathrm{X}_3^T (\boldsymbol{\phi}_3 \lambda_3 + \overline{\boldsymbol{\phi}_3}\,\overline{\lambda_3}) \tag{3.25}$$

$$\overline{\lambda_2} = \overline{\boldsymbol{\phi}_2^T} \mathrm{X}_3^T (\boldsymbol{\phi}_3 \lambda_3 + \overline{\boldsymbol{\phi}_3}\,\overline{\lambda_3}) \tag{3.26}$$

$$\begin{aligned} \lambda_3 = {} & \boldsymbol{\phi}_3^T \mathrm{X}_4^T (\boldsymbol{\phi}_4 \lambda_4 + \overline{\boldsymbol{\phi}_4}\,\overline{\lambda_4}) + \boldsymbol{\phi}_3^T \mathrm{X}_5^T (\boldsymbol{\phi}_5 \lambda_5 + \overline{\boldsymbol{\phi}_5}\,\overline{\lambda_5}) + \\ & \boldsymbol{\phi}_3^T \mathrm{X}_6^T (\boldsymbol{\phi}_6 \lambda_6 + \overline{\boldsymbol{\phi}_6}\,\overline{\lambda_6}) + \boldsymbol{\phi}_3^T \mathrm{X}_7^T (\boldsymbol{\phi}_7 \lambda_7 + \overline{\boldsymbol{\phi}_7}\,\overline{\lambda_7}) + \\ & \boldsymbol{\phi}_3^T \mathrm{X}_8^T (\boldsymbol{\phi}_8 \lambda_8 + \overline{\boldsymbol{\phi}_8}\,\overline{\lambda_8}) + \boldsymbol{\phi}_3^T \mathrm{X}_9^T (\boldsymbol{\phi}_9 \lambda_9 + \overline{\boldsymbol{\phi}_9}\,\overline{\lambda_9}) \end{aligned} \tag{3.27}$$

$$\begin{aligned} \overline{\lambda_3} = {} & \overline{\boldsymbol{\phi}_3^T} \mathrm{X}_4^T (\boldsymbol{\phi}_4 \lambda_4 + \overline{\boldsymbol{\phi}_4}\,\overline{\lambda_4}) + \overline{\boldsymbol{\phi}_3^T} \mathrm{X}_5^T (\boldsymbol{\phi}_5 \lambda_5 + \overline{\boldsymbol{\phi}_5}\,\overline{\lambda_5}) + \\ & \overline{\boldsymbol{\phi}_3^T} \mathrm{X}_6^T (\boldsymbol{\phi}_6 \lambda_6 + \overline{\boldsymbol{\phi}_6}\,\overline{\lambda_6}) + \overline{\boldsymbol{\phi}_3^T} \mathrm{X}_7^T (\boldsymbol{\phi}_7 \lambda_7 + \overline{\boldsymbol{\phi}_7}\,\overline{\lambda_7}) + \\ & \overline{\boldsymbol{\phi}_3^T} \mathrm{X}_8^T (\boldsymbol{\phi}_8 \lambda_8 + \overline{\boldsymbol{\phi}_8}\,\overline{\lambda_8}) + \overline{\boldsymbol{\phi}_3^T} \mathrm{X}_9^T (\boldsymbol{\phi}_9 \lambda_9 + \overline{\boldsymbol{\phi}_9}\,\overline{\lambda_9}) \end{aligned} \tag{3.28}$$

$$\lambda_4 = \boldsymbol{\phi}_4^T \mathcal{I}_4 a_4 \tag{3.29}$$

$$\overline{\lambda_4} = \overline{\boldsymbol{\phi}_4^T} \mathrm{I}_4 \mathrm{a}_4 \tag{3.30}$$

$$\lambda_5 = \boldsymbol{\phi}_5^T \mathcal{I}_5 a_5 \tag{3.31}$$

$$\overline{\lambda_5} = \overline{\boldsymbol{\phi}_5^T} \mathrm{I}_5 \mathrm{a}_5 \tag{3.32}$$

$$\lambda_6 = \boldsymbol{\phi}_6^T \mathcal{I}_6 a_6 \tag{3.33}$$

$$\overline{\lambda_6} = \overline{\boldsymbol{\phi}_6^T} \mathrm{I}_6 \mathrm{a}_6 \tag{3.34}$$

$$\lambda_7 = \boldsymbol{\phi}_7^T \mathcal{I}_7 a_7 \tag{3.35}$$

$$\overline{\lambda_7} = \overline{\boldsymbol{\phi}_7^T} \mathrm{I}_7 \mathrm{a}_7 \tag{3.36}$$

$$\lambda_8 = \boldsymbol{\phi}_8^T \mathcal{I}_8 a_8 \tag{3.37}$$

$$\overline{\lambda_8} = \overline{\boldsymbol{\phi}_8^T} \mathrm{I}_8 \mathrm{a}_8 \tag{3.38}$$

$$\lambda_9 = \boldsymbol{\phi}_9^T \mathcal{I}_9 a_9 \tag{3.39}$$

$$\overline{\lambda_9} = \overline{\boldsymbol{\phi}_9^T} \mathrm{I}_9 \mathrm{a}_9 \tag{3.40}$$

The force equations for the left and right translational masses (λ_5-λ_4, λ_7-λ_6, λ_9-λ_8) along the three principal axes can can be combined together because they are constrained to always be an equal distance away from the spherical joint. This means the masses have the same velocity and acceleration but in opposite directions. Substituting the constrained forces ($\overline{\lambda_n}$) into the unconstrained equations and simplifying

the results, leads to the following set of equations which are used to describe the nine degrees-of-freedom for the RMP model's motions,

$$\begin{aligned}
\boldsymbol{\tau}_\theta &= \boldsymbol{\phi}_1^T \mathrm{X}_2^T \mathrm{X}_3^T (\mathrm{X}_4^T \mathrm{I a}_4 + \mathrm{X}_5^T \mathrm{I a}_5 + \mathrm{X}_6^T \mathrm{I a}_6 + \mathrm{X}_7^T \mathrm{I a}_7 + \mathrm{X}_8^T \mathrm{I a}_8 + \mathrm{X}_9^T \mathrm{I a}_9) && (3.41)\\
\mathbf{f}_l &= \boldsymbol{\phi}_2^T \mathrm{X}_3^T (\mathrm{X}_4^T \mathrm{I a}_4 + \mathrm{X}_5^T \mathrm{I a}_5 + \mathrm{X}_6^T \mathrm{I a}_6 + \mathrm{X}_7^T \mathrm{I a}_7 + \mathrm{X}_8^T \mathrm{I a}_8 + \mathrm{X}_9^T \mathrm{I a}_9) && (3.42)\\
\boldsymbol{\tau}_\alpha &= \boldsymbol{\phi}_3^T (\mathrm{X}_4^T \mathrm{I a}_4 + \mathrm{X}_5^T \mathrm{I a}_5 + \mathrm{X}_6^T \mathrm{I a}_6 + \mathrm{X}_7^T \mathrm{I a}_7 + \mathrm{X}_8^T \mathrm{I a}_8 + \mathrm{X}_9^T \mathrm{I a}_9) && (3.43)\\
\mathbf{f}_x &= \boldsymbol{\phi}_4^T \mathrm{I}(\mathrm{a}_5 - \mathrm{a}_4) && (3.44)\\
\mathbf{f}_y &= \boldsymbol{\phi}_6^T \mathrm{I}(\mathrm{a}_7 - \mathrm{a}_6) && (3.45)\\
\mathbf{f}_z &= \boldsymbol{\phi}_8^T \mathrm{I}(\mathrm{a}_9 - \mathrm{a}_8) && (3.46)
\end{aligned}$$

where $\boldsymbol{\tau}_\theta$ is the 2D torque acting on the universal joint, $\mathbf{f}_l$ is the 1D force controlling the height of the RMP, $\boldsymbol{\tau}_\alpha$ is the 3D torque controlling the orientation of the ellipsoid using a spherical joint, and $\mathbf{f}_x$, $\mathbf{f}_y$, $\mathbf{f}_z$ are the 1D forces controlling the distance the point masses are from the spherical joint (see Figure 3.2).

The above equations account for the constraints and calculate the forces the RMP encounters based on its current state and the accelerations acting on it. However, the simulation environment used for predicting MIIs prescribes the joint forces and it is the accelerations that are unknown. Rearranging the equations to explicitly solve for the accelerations is difficult because of the constraints on the translational masses. In order to solve for the accelerations, the equations are formulated as a vector/matrix product using equations (3.1) and (3.2) as follows,

$$\mathbf{f} = \mathbf{M}\mathbf{A} + \mathbf{b} \tag{3.47}$$

where

$$\overbrace{\begin{bmatrix} \tau_{\theta_x} \\ \tau_{\theta_z} \\ f_l \\ \tau_{\alpha_x} \\ \tau_{\alpha_y} \\ \tau_{\alpha_z} \\ f_x \\ f_y \\ f_z \end{bmatrix}}^{\mathbf{f}} = \overbrace{\begin{bmatrix} M_{1,1} & M_{1,2} & \dots & M_{1,9} \\ M_{2,1} & M_{2,2} & \dots & M_{2,9} \\ M_{3,1} & M_{3,2} & \dots & M_{3,9} \\ M_{4,1} & M_{4,2} & \dots & M_{4,9} \\ M_{5,1} & M_{5,2} & \dots & M_{5,9} \\ M_{6,1} & M_{6,2} & \dots & M_{6,9} \\ M_{7,1} & M_{7,2} & \dots & M_{7,9} \\ M_{8,1} & M_{8,2} & \dots & M_{8,9} \\ M_{9,1} & M_{9,2} & \dots & M_{9,9} \end{bmatrix}}^{\mathbf{M}} \overbrace{\begin{bmatrix} a_1 \\ a_2 \\ a_3 \\ a_4 \\ a_5 \\ a_6 \\ a_7 \\ a_8 \\ a_9 \end{bmatrix}}^{\mathbf{A}} + \overbrace{\begin{bmatrix} b_1 \\ b_2 \\ b_3 \\ b_4 \\ b_5 \\ b_6 \\ b_7 \\ b_8 \\ b_9 \end{bmatrix}}^{\mathbf{b}}$$

The 9×1 vector $\mathbf{f}$ contains the forces for each joint in the RMP. The 9×9 matrix $\mathbf{M}$ collects the inertial terms for each joint, the 9×1 vector $\mathbf{A}$ contains the joint accelerations, and the 9×1 vector $\mathbf{b}$ has the link acceleration terms. The ship's accelerations are taken into account when calculating the $\mathbf{b}$ vector. Once the equations have been transformed into matrix form, they can be rearranged to solve for the acceleration vector by computing the inverse of the 9×9 $\mathbf{M}$ matrix yielding,

$$\mathbf{A} = \mathbf{M}^{-1}(\mathbf{f} - \mathbf{b}) \tag{3.48}$$

Equation (3.48) is used at every time-step to compute the accelerations of each of the joints in the RMP model. A fourth-order Runge-Kutta integrator with adaptive step size, as presented in Numerical Recipes in C++ [53], is used to advance the simulation time and update the pendulum's velocities and accelerations.

3.5 RMP Summary

To summarize, the equations-of-motion developed in Section 3.4 form the basis of a dynamic simulation used for modeling the motions of a Reaction Mass Pendulum and enable the prediction of Motion Induced Interruptions. In the next chapter, the algorithms used to control the RMP model using an ankle/hip strategy are presented.

Chapter 4

Ankle/Hip Control Strategy

4.1 Introduction

The following chapter presents an ankle/hip control strategy that was used to maintain postural stability for the RMP model. The algorithm is based on an ankle/hip strategy presented by Kiemel [28]. The algorithm was originally used on a 2D planar Inverted Pendulum plus Flywheel Model (IPFM) and was modified for this research to work with a 3D RMP model. Kiemel demonstrated that, for the IPFM, the ankle/hip strategy could withstand a 33.6% larger disturbance than an ankle strategy alone.

The next section introduces the notion of an Instantaneous Capture Point (ICP) which is used to control the location of the Centre of Pressure (COP). Next, Virtual Model Control (VMC) is presented which is used to determine the joint torques required to keep the model upright. Finally, the balance control algorithm is introduced and each component of the controller is elaborated on.

4.1.1 ICP Calculation

The ICP is the point on the ground plane where the COP should be located to bring the model to a stop with the Center of Mass (COM) directly over the COP [45] [47]. The location of the ICP is constrained to be within the support region, where the support region is a rectangle on the ground defined by the model's foot stance (see Figure 4.1). When the location of the ICP falls outside of the support region, the control algorithm switches from an ankle strategy to an ankle/hip strategy and an MII is signaled. The ICP is a function of the position and velocity of the COM.

The location of the ICP determines how close the model is to falling. When the ICP falls outside of the support region the model is unstable and an MII is detected. Controlling the location of the ICP is critical to keeping the model upright. The

current kinematic and dynamic state of the system is used to determine the position and velocity of the COM. The ICP position is calculated using the following equations:

$$ICP_x = COM_x + \dot{COM}_x\sqrt{\frac{h}{g}}$$

$$ICP_z = COM_z + \dot{COM}_z\sqrt{\frac{h}{g}}$$

where g is the gravitational constant and h is the height of the COM.

ICP_y is the y coordinate on the ground plane where ICP_x and ICP_z meet. The calculated ICP position is then used to calculate the desired location of the centre-of-pressure.

4.1.2 ICP Control

The basis for the control algorithm is controlling the position of the ICP which is carried out simultaneously with the upper body orientation control, introduced in the next section. The ICP is kept within the support region by modulating the position of the desired COP. The location of the desired COP is calculated in such a way that the ICP is always between the desired COP and the desired ICP. This causes the ICP to move towards the desired ICP location. The desired location of the COP is calculated using the following formula:

$$COP_{des} = ICP - K_p\left(ICP_{des} - ICP\right) \tag{4.1}$$

where ICP is the current location of the ICP, ICP_{des} is the desired location of the ICP, and K_p is the proportional gain.

The formula places the COP in line with the ICP and the desired ICP location as shown in Figure 4.1. The COP cannot fall outside of the support region. If the desired COP location does lie outside the region, it is projected to the edge of the support polygon.

The ICP controller only has one proportional gain but it can be considered a PD-controller because both the position and velocity of the COM are used in the calculation. The gain is kept the same for both the ankle strategy and the ankle/hip strategy.

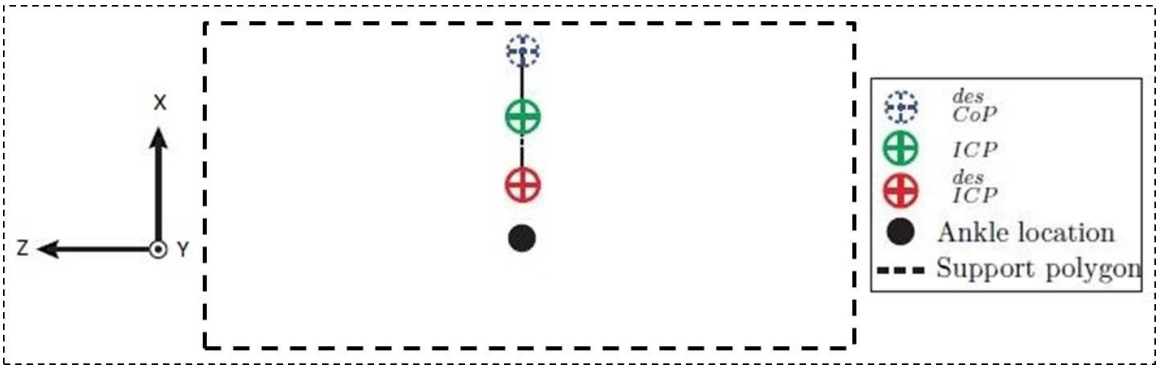

Figure 4.1: A top-down view of the support region [28]. The region is defined by a double foot support stance where the feet are parallel and about shoulder width apart for an average human. The COP pushes the ICP towards the desired ICP location.

4.2 Virtual Model Control

When the ICP leaves the support region, an ankle/hip strategy is used. This requires the upper body to generate a large enough angular acceleration to push the ICP back inside the support polygon. To keep the model from exceeding joint limits, the velocity of the COM also has to be decelerated. This could be accomplished using two Proportional Derivative (PD) controllers but that would require tuning four gains which can be a delicate processes to get the two to cooperate. As well, the gains would most likely be dependent on the magnitude of the disturbance. An alternate approach, which was used in this research, is to use VMC [46].

VMC uses virtual forces to generate desired joint torques. The virtual forces have the same effect as physically applying desired joint torques. VMC is more desirable than PD control in this instance because the effects of parameter changes on VMC can be predicated more easily [47] making tuning simpler. Instead of using an inverse dynamics approach, as is done in PD control, VMC calculates the Jacobian (inverse kinematics) of the model to determine the torques at the joints. The joint torques can be calculated using the following equation:

$$\boldsymbol{\tau} = {}^{A}_{B}\mathrm{J}^{T}\mathbf{W} \tag{4.2}$$

where $\boldsymbol{\tau}$ is a vector of joint torques, ${}^{A}_{B}\mathrm{J}^{T}$ is the transpose of the model's Jacobian matrix from frame A to frame B, and W is the vector of applied virtual forces (wrench) on the model at frame B.

The VMC algorithm considers the model as a whole rather than on an individual joint level. The goal is to come up with upper body forces that can be transformed, using VMC, into individual joint torques for the entire model. In the sagittal plane (see Figure 4.2), there are three virtual forces calculated for the trunk: τ_{tr_z}, a virtual torque on the upper body; f_x, a horizontal virtual force; and f_z, a vertical virtual force. These three forces are combined in the wrench vector and can be written as:

$$\mathbf{W} = \begin{bmatrix} f_x \\ f_y \\ \tau_{tr_z} \end{bmatrix} \tag{4.3}$$

A similar formulation is used for the frontal plane. The virtual forces are applied on the trunk for both the ankle strategy and the hip strategy. The way in which the virtual torque, τ_{tr}, is calculated switches dependent on the current strategy being applied, as discussed in Section 4.3.1.

4.3 RMP Control Strategy

As stated above, the RMP model uses VMC to determine virtual forces on the upper body and converts those forces to physical joint torques using equation (4.3). The ankle/hip control algorithm is summarized in Figure 4.3. The algorithm consists of five main components, as indicated by the numbers in the figure:

1. Instantaneous Capture Point (ICP) calculation
2. Instantaneous Capture Point (ICP) control
3. Upper body orientation control
4. Gravity compensation
5. Joint torque calculation

The five components defining the control algorithm will be detailed in the following subsections.

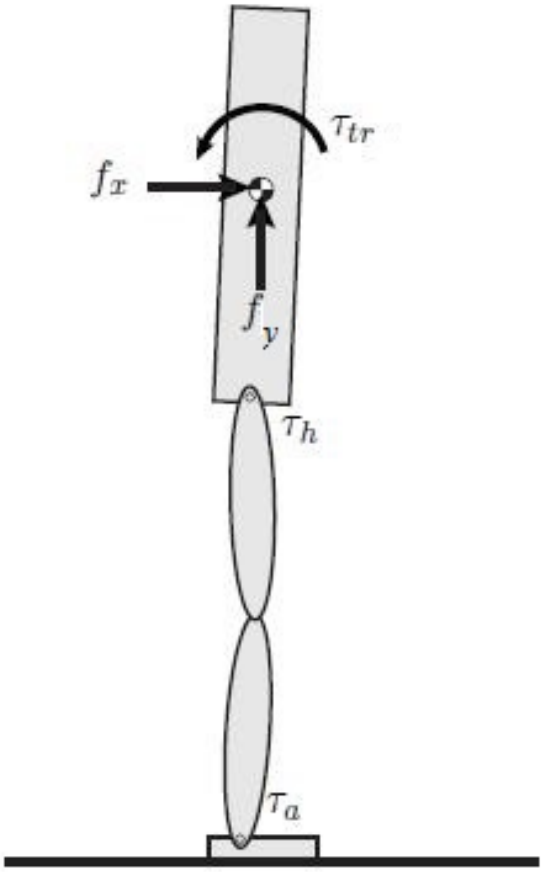

Figure 4.2: VMC in the sagittal plane. [28] The virtual forces consist of a virtual torque on the upper body (τ_{tr}), a virtual horizontal force (f_x), a virtual vertical force (f_z). The three virtual forces are transformed into two joint torques using VMC: the ankle torque (τ_a) and the hip torque (τ_h)

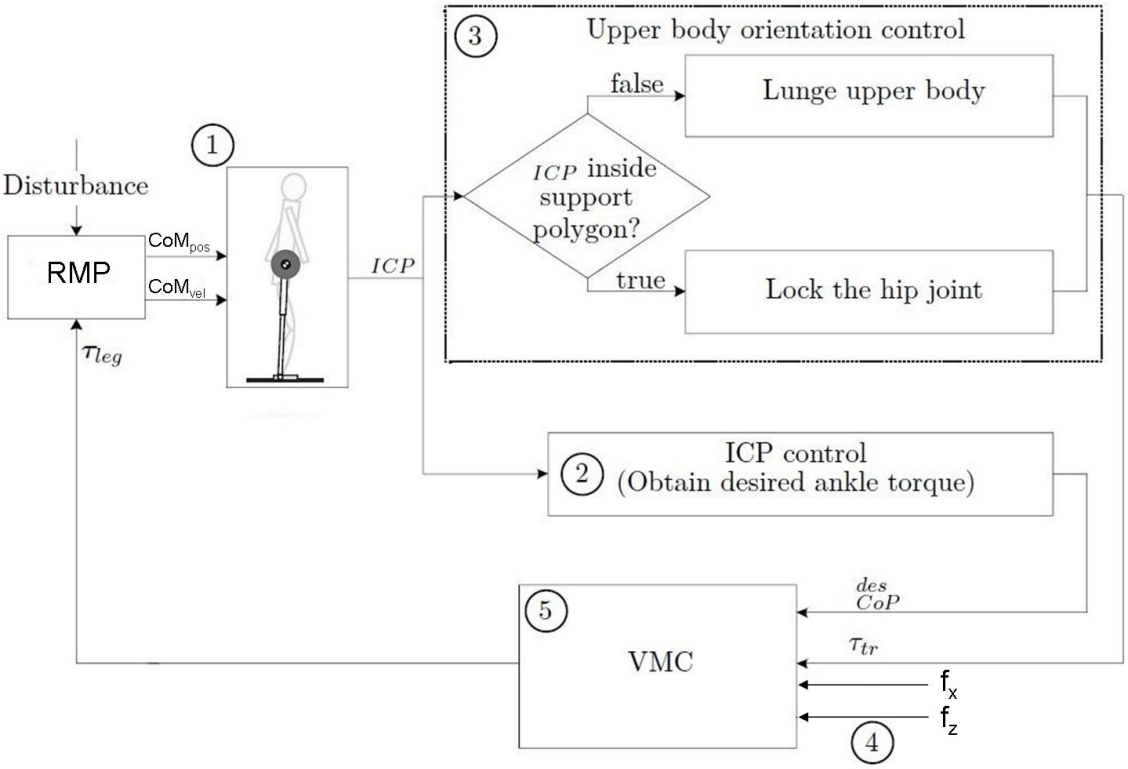

Figure 4.3: Ankle/Hip Strategy Overview [28]: (1) The ICP is calculated using the position and velocity of the centre-of-mass. (2) The ICP controller determines where the COP should be placed to move the ICP to its desired location. (3) If the ICP is inside the support region, the hip-joint is locked. If the ICP is outside the support region, a virtual torque is applied to the hip-joint causing a lunging motion which pushes the ICP back inside the support region. (4) A constant vertical virtual force f_z is applied to compensate for the gravitational pull on the model. (5) Virtual Model Control (VMC) is used to calculate the actual torques to be applied to the RMP model.

4.3.1 Upper Body Orientation Control

The upper body's orientation is controlled by applying a virtual torque, τ_{tr}, to the trunk. This regulates the pitch angle of the upper body and is carried out in parallel with the ICP control. There are two modes of operation, dependent on the current location of the ICP. If the ICP location lies inside the support polygon, it freezes the spherical joint to a desired orientation using a PD-controller. If a large disturbance is encountered which moves the ICP outside of the support region, a virtual torque is applied to the spherical joint, causing a lunging motion in the direction of the disturbance. Further details on each of the control strategies can be found below.

Locking the hip

The objective of this strategy is to keep the upper body at a fixed orientation. This is achieved using a proportional derivative controller on the spherical joint of the RMP model. The PD-controller uses the following equation:

$$\boldsymbol{\tau_{tr}} = K_p \left(\boldsymbol{q^{dif}}\right) + K_d \left(\boldsymbol{\dot{q}_{des}} - \boldsymbol{\dot{q}}\right) \tag{4.4}$$

where $\boldsymbol{\tau_{tr}}$ is a 3×1 virtual torque vector on the upper body, K_p is the proportional gain, $\boldsymbol{q^{dif}}$ is the distance between the desired and current angle of the spherical joint, K_d is the derivative gain, $\boldsymbol{\dot{q}_{des}}$ is the desired velocity of the spherical joint (always set to 0 for the RMP model), and $\boldsymbol{\dot{q}}$ is the current velocity of the spherical joint.

Because the orientation of the upper body is represented as a quaternion, comparing the difference between the desired location and the current location cannot be done by a simple subtraction. Instead the following formula is used to compute the distance between two quaternions [57]:

$$\boldsymbol{q^{dif}} = q_{\varphi}^{des} \begin{bmatrix} q_x \\ q_y \\ q_z \end{bmatrix} - q_{\varphi} \begin{bmatrix} q_x^{des} \\ q_y^{des} \\ q_z^{des} \end{bmatrix} - \begin{bmatrix} q_x^{des} \\ q_y^{des} \\ q_z^{des} \end{bmatrix} \times \begin{bmatrix} q_x \\ q_y \\ q_z \end{bmatrix}$$

where $\boldsymbol{q^{dif}}$ is a 3×1 vector, q_{φ}^{des} is the φ component of the desired orientation quaternion, $\begin{bmatrix} q_x \\ q_y \\ q_z \end{bmatrix}$ is a 3×1 vector containing the x, y, z parameters of the current

orientation quaternion, q_φ is the φ component of the current orientation quaternion, and $\begin{bmatrix} q_x^{des} \\ q_y^{des} \\ q_z^{des} \end{bmatrix}$ is a 3×1 vector containing the x, y, z parameters of the desired orientation quaternion.

Lunging the upper body

The objective of this strategy is lunge the upper body in the direction of the disturbance. This is triggered when the ICP leaves the support region. The desired location of the COP is placed on the edge of the support polygon and a maximum amount of ankle torque is applied. The ankle torque alone will not be enough to move the ICP back into the support region. Therefore a large torque is applied to the upper body to create a rotational acceleration in the direction of the ICP. The torque causes a lunging action and moves the ICP back into the support polygon. A P-controller is used to calculate the desired torque on the upper body as follows:

$$\boldsymbol{\tau_{tr}} = K_p(\mathbf{ICP_{des}} - \mathbf{ICP})$$

where $\boldsymbol{\tau_{tr}}$ is a 3×1 virtual torque vector on the upper body, K_p is the proportional gain, $\mathbf{ICP_{des}}$ is the desired location of the ICP and $\mathbf{ICP}$ is the current location of the ICP.

The lunging motion causes the ICP to be pushed back towards the support region. As the location of the ICP gets closer to the support polygon, the distance between the desired and current location of the ICP decreases causing the torque to decrease as well. A threshold is set which determines if the ICP is far enough inside the support region to switch back to an ankle strategy. This is done to prevent the controller from getting stuck on the edge of the support boundary.

4.3.2 Gravity Compensation

In order to compensate for the gravitational force pulling down on the COM for the RMP model, a constant virtual vertical force f_y is always applied. The force is calculated as follows:

$$f_y = mg$$

where m is the total mass of the RMP model and g is the gravitational acceleration. This force also has the effect of decelerating the upper body when the ICP falls outside the support region. This virtual vertical force along with the hip torque, τ_{tr}, and the virtual horizontal forces f_x, f_z are used to calculate the actual joint torques applied to the RMP model using VMC.

4.3.3 Joint Torque Calculation

Once the following information is known:

1. desired location of the COP
2. the virtual vertical force to keep the COM at a defined height
3. the virtual torque on the upper body to keep it at a desired orientation

the ankle torques in the sagittal and frontal planes can be calculated to move the center-of-pressure to the prescribed location.

Virtual forces in the sagittal and frontal planes are calculated by using Virtual Toe Points (VTPs) [48]. A VTP represents a spot on the foot where no torque is applied in the horizontal plane. It acts like a joint on the foot but is not modeled as an actual joint on the physical model. The VTP is placed at the location of the desired center-of-pressure and its joint angle is set to zero. The location of the VTP changes over time as the location of the desired centre-of-pressure changes. The forward kinematic relationships between the joints of the model and the VTP is represented using a Jacobian matrix,

$$\begin{matrix} A \\ B \end{matrix}\mathrm{J} = \begin{bmatrix} J_{1,1} & J_{1,2} \\ J_{2,1} & J_{2,2} \\ 1 & 1 \end{bmatrix}$$

with

$$\text{Sagittal Plane} \begin{cases} J_{x_{1,1}} = & -l_{vtp_x}\cos\left(\varphi_{vtp_x}\right) + r_l\cos\left(\varphi_{vtp_x}+\theta_x\right) \\ J_{x_{1,2}} = & r_l\cos\left(\varphi_{vtp_x}+\theta_x\right) \\ J_{x_{2,1}} = & -l_{vtp}\sin\left(\varphi_{vtp_x}\right) + r_l\sin\left(\varphi_{vtp_x}+\theta_x\right) \\ J_{x_{2,2}} = & r_l\sin\left(\varphi_{vtp_x}+\theta_x\right) \end{cases}$$

$$\text{Frontal Plane} \begin{cases} J_{z_{1,1}} = & l_{vtp_z}\sin\left(\varphi_{vtp_z}\right) - r_l\sin\left(\varphi_{vtp_z}+\theta_z\right) \\ J_{z_{1,2}} = & -r_l\sin\left(\varphi_{vtp_z}+\theta_z\right) \\ J_{z_{2,1}} = & l_{vtp_z}\cos\left(\varphi_{vtp_z}\right) - r_l\cos\left(\varphi_{vtp_z}+\theta_z\right) \\ J_{z_{2,2}} = & -r_l\cos\left(\varphi_{vtp_z}+\theta_z\right) \end{cases}$$

where φ_{vtp} is the angle of the VTP, l_{vtp} is the length of the VTP, r_l is the height of the COM, θ_x if the angle of the ankle joint in the x axis, and θ_z is the angle of the ankle joint in the z axis.

Equation (4.2) is used to relate the virtual forces and the joint torques using a Jacobian matrix,

$$\tau = {}^{A}_{B}\mathrm{J}^{T}\mathbf{W}$$

where $\tau = \begin{bmatrix}\tau_a & \tau_h\end{bmatrix}^T$ are the joint torques, ${}^{A}_{B}\mathrm{J}$ is the Jacobian, and $\mathrm{W} = \begin{bmatrix}f_x & f_z & \tau_{tr}\end{bmatrix}^T$ is the wrench consisting of the virtual forces. This can be represented by the following matrix equations,

Sagittal Plane:

$$\begin{bmatrix}\tau_{a_x} \\ \tau_{h_x}\end{bmatrix} = \begin{bmatrix}J_{x_{1,1}} & J_{x_{2,1}} & 1 \\ J_{x_{1,2}} & J_{x_{2,2}} & 1\end{bmatrix}\begin{bmatrix}f_z \\ f_y \\ \tau_{tr_x}\end{bmatrix} \tag{4.5}$$

Frontal Plane:

$$\begin{bmatrix}\tau_{a_z} \\ \tau_{h_z}\end{bmatrix} = \begin{bmatrix}J_{z_{1,1}} & J_{z_{2,1}} & 1 \\ J_{z_{1,2}} & J_{z_{2,2}} & 1\end{bmatrix}\begin{bmatrix}f_x \\ f_y \\ \tau_{tr_z}\end{bmatrix} \tag{4.6}$$

where τ_{a_x} is the ankle torque in the x axis, τ_{a_z} is the ankle torque in the z axis, τ_{h_x} is the hip torque in the x axis, τ_{h_z} is the hip torque in the z axis, f_y is the virtual

vertical force in the y axis, f_x is the virtual horizontal force in the x direction, f_z is the virtual horizontal force in the z direction, τ_{tr_x} is the virtual trunk torque in the x axis, and τ_{tr_z} is the virtual trunk torque in the z axis.

The virtual horizontal forces, f_z and f_x are calculated using the following equations [28]:

$$f_z = -\begin{bmatrix} \frac{J_{x_{1,2}}}{J_{x_{1,1}}} & \frac{1}{J_{x_{1,1}}} \end{bmatrix} \begin{bmatrix} f_y \\ \tau_{tr_x} \end{bmatrix} \tag{4.7}$$

$$f_x = -\begin{bmatrix} \frac{J_{z_{1,2}}}{J_{z_{1,1}}} & \frac{1}{J_{z_{1,1}}} \end{bmatrix} \begin{bmatrix} f_y \\ \tau_{tr_z} \end{bmatrix} \tag{4.8}$$

Once the virtual horizontal forces, f_z and f_x, are calculated they can be substituted back into equation (4.5) and equation (4.6) respectively.

4.4 Model and Controller Parameters

The mass used for the RMP model is 78kg which is divided into six equal parts for each of the six point masses. The height of the COM for the model is initialized to 87cm. The lengths along the three principal axes which define the ellipsoid that represents the upper body are set to 25cm, 60cm, and 25cm respectively (See Figure 4.4).

The K_p parameter used in equation (4.1) is set to 0.78. The K_p parameter used in equation (4.4) is 240 and the K_d parameter is 90. The torque limit for the ankle joint is set to 237N.

4.5 Implementation Details

The RMP model and the ankle/hip controller were implemented on an Intel(R) Core(TM) i7-4800MQ CPU running at 2.70GHz under a Windows 7, 64-bit operating system. The software was implemented in Microsoft Visual Studio 2010 using C++ and OpenGL.

4.6 Controller Summary

This chapter has presented the algorithms used to control the RMP model. Virtual Model Control was used which computes virtual forces on the upper body to move

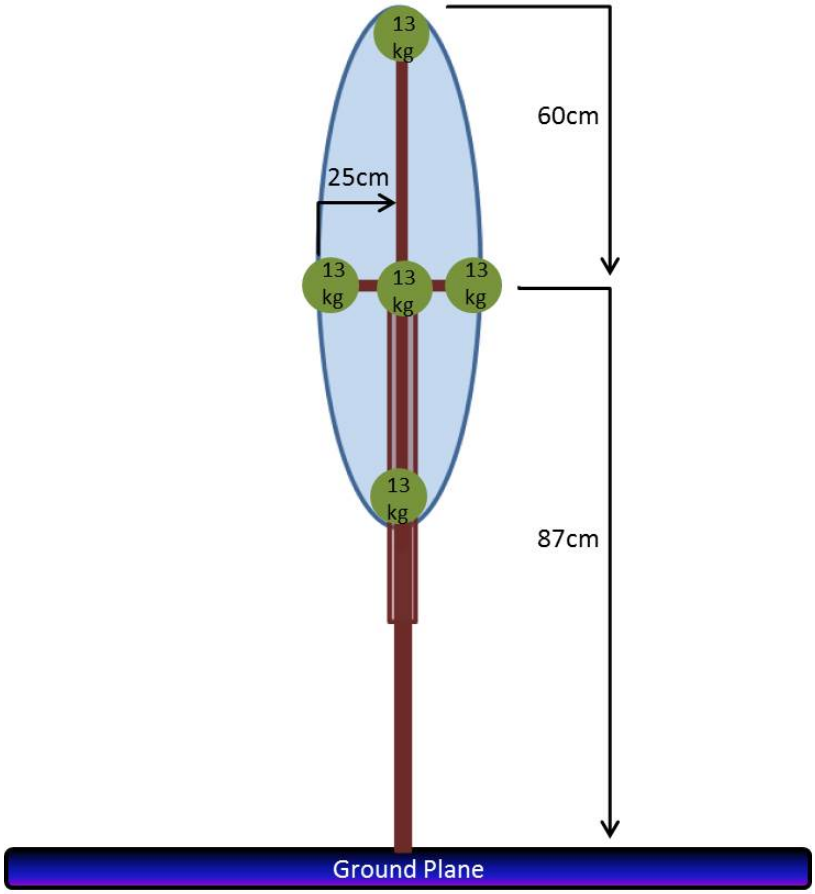

Figure 4.4: Side view of the RMP model. The mass of the model is 78kg, divided between six point masses evenly. The height of the centre-of-mass is 87cm. The lengths along the three axes defining the ellipsoid of the upper body are 25cm, 60cm, and 25cm.

the ICP to a desired spot. The motion of the ICP causes the centre-of-pressure to be 'pushed' to a specified location. If the centre-of-pressure is within the support polygon, then only ankle toque is used to keep the model upright. If the centre-of-pressure falls outside the base of support, then the upper body is lunged to try and bring the centre-of-pressure back inside the base.

The next chapter will detail how the model was validated to predict MIIs using recent sea trial data.

Chapter 5

Model Validation

5.1 RMP Validation Approach

The RMP model was run in two configurations to predict MII times. In one configuration, the distance of all the point masses from the COM were set to zero. This reduces the RMP model to an Inverted Pendulum (IP) (see Figure 5.1 - left) with a two degree-of-freedom universal joint at the 'ankle'. When run in this manner, the controller only uses an ankle strategy to maintain balance, similar to the model used by Langlois et al. [32]. The second configuration (see Figure 5.1 - right) positioned the point masses as described in Section 4.4. The controller uses an ankle/hip strategy in this configuration. The predicted MIIs for these two configurations of the RMP model are compared to MIIs observed during a sea trial conducted in 2012.

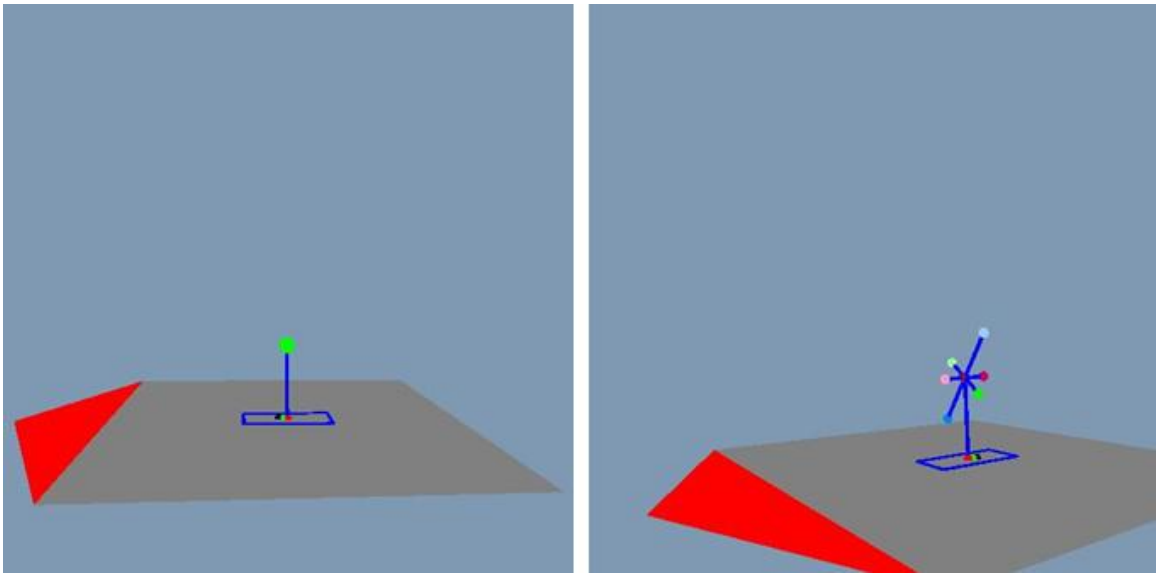

Figure 5.1: IP Model (left) and RMP model (right)

5.2 Controller Tuning

MII data for participant Q3 was used when tuning the controller because it contained the greatest number and variety of observed MIIs. When the model was run in the RMP configuration, the gains for the seven PD controllers for the prismatic joints were chosen to maintain stability while also ensuring the distance of each joint was kept close to the desired value. For the height of the COM the distance was maintained at 78cm and the X, Y, and Z distances along the principal axes were kept to 25cm, 60cm, and 25cm respectively. For the spherical joint, a PD controller was also used to keep the upper body at a desired orientation.

The proportional gain for the desired COP calculation was varied to measure its effect on the number of MIIs predicted. The higher the gain value, the further the desired COP was from the current ICP location. An initial gain was chosen and the model was run to predict the number of MIIs. The predicted MIIs were compared to the observed MIIs and the number of identified, correct, false positive and false negative MIIs were recorded. The initial gain would then be doubled to see if the predictions would get better or worse. The initial gain would also be halved to see if the predictions got better or worse. This process of increasing or decreasing the gain continued until a gain was found that gave the best overall predictions for the Q3 participant. Once the optimal gain was found the model was run to predict MIIs for the remaining participants.

When the model was run in the IP configuration, the same gains were used for the prismatic joints but this time the distances maintained were 78cm for the COM and 0cm along all the principal axes. In the IP configuration, there was no need to control the upper body, so no forces were generated for the spherical joint. The Q3 participant was used again for initially predicting the MIIs and once the gain was chosen for the desired COP calculation, the MIIs for the remaining participants were calculated.

5.3 MII Data Collection

MII and ship motion data from a DRDC sea trial was used to validate our model. A description of the how the data was collected can be found in Appendix B. A

detailed list of when MIIs were identified and the MII predictions from the RMP and IP models can be found in Appendix C. The motion capture data for participant Q5 was corrupted so no MIIs could be validated for them. As well, the ship motion data was corrupted for participant D1 and their MIIs could also not be validated.

5.4 Experimental Sessions

During the DRDC sea trial, each participant was allocated a 90-minute session to collect their postural stability data. They stood in a T-pose with their feet parallel and about shoulder width apart and stomped their foot to mark the start of the leg. Then they performed a data entry exercise using a pen and paper for five minutes (see Figure 5.2) while facing towards the front of the ship. After five minutes they reset back to their starting T-pose position and stomped their foot before they turned forty-five degrees towards the port side and continued to manually enter data. Once another five minutes had elapsed they once again reset back to the original T-pose position, stomped their foot, and turned to the port side and continued entering data manually for another five minutes. This process was repeated for a second time but now a tablet computer was used when entering data rather then a pen and paper.

5.5 MII Identification

Once the motion capture data is post processed and exported into a format suitable for playback, it is viewed in real-time. When a participant is observed to make a postural adjustment, the time of the occurrence is manually recorded. A postural adjustment might include taking a step, flailing the arms, or a sudden change in posture. It is a subjective observation at times and is not necessarily the result of the dynamics of the system.

Once the data for each participant's five-minute orientation run was examined to identify MII times, the ship motion data that occurred during that trial run was extracted and saved to another file for input into the RMP and IP simulations. The RMP and IP simulations use the ship's dynamics to predict MIIs and record the time of occurrence. In the RMP simulation, an MII occurs when a hip and ankle strategy is required to maintain balance. When the MII time identified in the motion capture

Figure 5.2: Participant performing manual data entry.

data is within a five second window of the time predicted by the RMP or IP model, the two are said to agree. A five second window was used for two reasons. First, the identified MII time was not exact so some leeway is needed. Second, once the RMP or IP model identifies an MII it is unbalanced and the controller is given five seconds to try and get the pendulum back into a stable state before it tries to identify the next MII. The state is said to be stable if the controller is able to maintain postural stability using just an ankle strategy and the COM is within the support region.

In the IP simulation, whenever the ICP fell outside the support region an MII was detected. In this configuration, when the ankle torque is insufficient to maintain the COM inside the base of support there is no way for the controller to bring the model back to a stable state. In these situations the model parameters are reset to its initial state to force the model back to a stable configuration.

5.6 IP and RMP MII Predictions

This section presents the results of the IP and RMP models' MII predictions for the eight participants used in the study. Table 5.1 shows a summary of the MII predictions for the IP model and Table 5.2 shows a summary of the predictions for the RMP model. For a complete list of actual MII times versus predicted MII times see Appendix C. The columns of the table have the following format:

- **Par ID** - Participant ID
- **# Ident** - Total number of observed MIIs for this participant
- **# Pred** - Total number of MIIs predicted for this participant by the controller
- **# FP** - Number of false positive results
- **# FN** - Number of false negative results
- **# Cor** - Number of correctly predicted MIIs
- **% Cor** - The percentage of MIIs correctly predicted

A False Positive is defined to be an MII predicted by the IP model that was not identified in the motion capture data. A False Negative is defined to be an identified MII from the motion capture data that was not predicted by the IP model. Because a five second window is used when identifying MIIs (see Section 5.5), a single predicted MII may map to multiple actual MIIs.

Table 5.1: IP MII Results by Participant

Par ID	# Ident	# Pred	# FP	# FN	# Cor	% Cor
Q1	1	0	0	1	0	0.0%
Q2	4	7	5	2	2	50.0%
Q3	70	70	19	30	40	57.1%
Q4	0	0	0	0	0	—
Q6	9	6	3	7	2	22.2%

Continued on next page

Table 5.1 – *Continued from previous page*

Par ID	**# Ident**	**# Pred**	**# FP**	**# FN**	**# Cor**	**% Cor**
Q7	1	0	0	1	0	0.0%
D2	5	12	9	2	3	60.0%
D3	23	18	11	14	9	39.1%
Total	113	113	47	57	56	49.6%

Table 5.2: RMP MII Results by Participant

Par ID	**# Ident**	**# Pred**	**# FP**	**# FN**	**# Cor**	**% Cor**
Q1	1	0	0	1	0	0.0%
Q2	4	1	1	4	0	0.0%
Q3	70	79	28	16	54	71.1%
Q4	0	0	0	0	0	—
Q6	9	5	1	3	6	66.7%
Q7	1	0	0	1	0	0.0%
D2	5	23	18	1	4	80.0%
D3	23	15	4	12	11	47.8%
Total	113	123	52	38	75	66.4%

Total MII Predictions

As can be seen from Tables 5.1 and 5.2, the IP model was able to predict MII occurances with an accuracy of about 50% while the RMP model was able to predict MII occurrences with an accuracy of about 66% for this data set. The IP model correctly predicted the total number of MIIs while the RMP model over-predicted the total number of MIIs by about 9%.

Table 5.3: IP/RMP - False Positives and False Negatives by Percentage

Model	FP Percentage	FN Percentage
IP	42.6%	50.4%
RMP	42.3%	33.6%

Of the 113 MIIs predicted by the IP model, 42.6% did not match an MII identified in the motion capture data. Of the 113 MIIs identified in the motion capture data, the IP model was unable to identify 50.4% of them (See Table 5.3).

Of the 123 MIIs predicted by the RMP model, 42.3% did not match an MII identified in the motion capture data. Of the 113 MIIs identified in the motion capture data, the RMP model was unable to identify 33.6% of them (See Table 5.3).

For this set of trial data, the RMP model with an ankle/hip controller was able to correctly predict MIIs with about 34% greater accuracy than the IP model which only used an ankle strategy for postural stability.

5.7 Results Discussion

In 2009, Langlois et al. [32] performed a similar experiment with twelve participants, also onboard the CFAV Quest. Platform motions were recorded in six degrees-of-freedom and they were synchronized to observed MII events. That data was then used to calibrate a planar inverted pendulum model to predict MII events. Similar sea conditions (2-5 metre significant wave heights) were encountered in the 2009 trial and a similar number of MII events were observed as can be seen in Table 5.4. The IP model with two degrees-of-freedom at the 'ankle' joint performed about 9 percentage points better than the one degree-of-freedom IP model used in the 2009 trial while the RMP model, using an ankle/hip controller, showed an improvement of about 25 percentage points over the planar inverted pendulum model.

Table 5.4: Langlois et al. MII Predictions from 2009

Total Identified	**Total Predicted**	**Total Correct**	**Percentage Correct**
134	134	55	41.0%

More testing is needed to further compare these three approaches of MII prediction, especially at higher sea-states. Sea trial data provides a realistic environment for observing MIIs but it is impossible to reproduce the exact conditions that occurred during the data collection. There are many statistical factors that influence the accuracy of predicting MIIs using sea trial data such as the significant wave heights encountered, the height/weight variations of the participants, the experience of the sailors, and environmental factors. For these reasons, the more MII data collected in various conditions, the more accurate the statistical model becomes. While this one sea trial probably does not provide enough statistical data to accurately describe the effectiveness of the RMP model, the initial results do look promising.

The next chapter will present a discussion of the conclusions of this thesis and outline areas of future research.

Chapter 6

Conclusions and Future Work

The goal of this thesis was to develop a physics based, humanoid model which could predict MII occurrences and in the future be used to visualize seakeeping tasks. Another approach that can be used to predict MIIs are statistical methods such as those introduced by Graham et al. [17], Crossland et al. [7] [8] [10], Gehl [15], or Crossland et al. [9]. A physics based approach was chosen over a statical approach because it is easier to integrate it into a physics based ship motion simulation and it can be used to visualize humanoid motions.

The model was validated using real-world data of observed MIIs at sea. This was accomplished by modifying Lee and Goswami's [33] RMP model to have a six degree-of-freedom joint at the base to represent a moving ship deck. In order to generate joint torques for the model and predict when an MII would occur, an ankle/hip controller was used. The controller was based on a 2D version presented by Kiemel [28]. It was modified to work in 3D on a moving platform and use an RMP model rather than a 2D planar IPFM.

Sea trial data from 2012, where motion capture data was collected for human participants performing a quiet standing exercise, was used to validate the RMP model.

For the sea trial data collected, the RMP model was able to predict MIIs with 66% accuracy while the IP model had an accuracy of about 50%. These were an improvement over a similar sea trial in 2009 where a planar inverted pendulum model was used to predict MIIs with 41% accuracy. The 3D IP model showed an improvement of about 9 percentage points over the planar IP model. The RMP model showed an improvement of about 25 percentage points over the planar IP model. The RMP and IP models can only predict MIIs caused by the actual forces acting on the participants at the time of the trial. MIIs can occur for many reasons and not all of them are the result of physical forces. Some other factors that can influence MIIs include, sea

sickness, fatigue, experience, or amount of sleep to name but a few.

The results of this thesis show that modeling postural stability with a more sophisticated model than the inverted pendulum may require more tuning because of the extra degrees-of-freedom but may be capable of better MII predictions because of its more accurate representation of human dynamics. More data is required to ensure the RMP model doesn't suffer from over-fitting the predictions to the observed data. For this research, a small number of participants were used and a limited number of MIIs were observed because of the lower sea states encountered. This makes it difficult to separate training data during the model tuning process. If more data was available, a set of training data could be used for tuning the model. Another advantage of the RMP model is it makes a better choice for motion re-targeting because it uses twelve degrees-of-freedom where as the IP model only uses three. Motion re-targeting is when a model with fewer degrees-of-freedom is mapped to a kinematic model with a higher degree of articulation.

Future Work

While the results of this research are promising, more data should be used to validate the RMP model further. This should include more sea trials and laboratory experiments because of the statistical component in the analysis arising from variability in sea conditions and subjects.

Lee and Goswami's [33] paper described a method to map the degrees-of-freedom for the RMP model to a humanoid model with higher degrees-of-freedom. This allowed them to animate a robot with 27 degrees-of-freedom using the RMP model which had only 12 degrees-of-freedom. This could be used to animate a more realistic character standing on a ship deck for higher fidelity visual simulations.

Another area that could be explored further would be to look at modeling stepping motions. When deck motions are large, a person tends to adjust their stance in order to maintain balance. This could be achieved through redefining the shape of the support region when an MII occurs or perhaps by combining two RMP models. Lee and Goswami [34] describe an approach to human gait control using an RMP model that could be adapted for stepping motions at sea.

This research only looked at quiet standing activities on a moving platform. It would be useful to examine more complex shipboard activities, such as those involved when a sailor is required to hold a tag line. The forces on the tag line will create an external pulling force on the person holding the line. These conditions occur in activities such as replenishment at sea, launch and recovery of small craft, or when moving loads with a crane. Modeling walking on a moving platform would also be an area for interesting analysis.

Appendix A

3D Vector as a Cross Product Matrix

Let vector $\boldsymbol{m}$ be a three-dimensional vector such that

$$\boldsymbol{m} = \begin{bmatrix} m_1 \\ m_2 \\ m_3 \end{bmatrix}$$

The cross product of $\boldsymbol{m}$ with another three-dimensional vector $\boldsymbol{n}$ can be written as the 3×3 matrix $\tilde{\mathrm{m}}$ multiplied by the 3×1 vector $\boldsymbol{n}$ where

$$\boldsymbol{m} \times \boldsymbol{n} = \tilde{\mathrm{m}}\mathbf{n} = \begin{bmatrix} 0 & -m_3 & m_2 \\ m_3 & 0 & -m_1 \\ -m_2 & m_1 & 0 \end{bmatrix} \begin{bmatrix} n_1 \\ n_2 \\ n_3 \end{bmatrix}$$

Appendix B

Data Collection

B.1 Introduction

This appendix describes the data that was collected during the Q-348 sea trial onboard DRDC's research ship, Canadian Forces Axillary Vessel (CFAV) Quest (Figure B.1). The nine day experiment was conducted from November 20th through November 28th of 2012. The research was a collaborative effort between scientists at DRDC Atlantic and Carleton University.

Figure B.1: DRDC's research vessel CFAV Quest (photo by Michael Martin)

Postural stability and cognitive efficiencies were measured during 90-minute sessions for thirteen participants. There were ten experienced sailors and three participants who were not familiar with being at sea. The subjects were asked to maintain balance in several orientations relative to the centerline of the ship and perform a

cognitive task. One task involved manually logging data on a clip board with pen and paper. The other task used a tablet computer to log the data. The motions of the ship and the participants were recorded.

B.2 Data Collection

This sections provides details on how the ship's motion data and the subjects' motion data were recorded.

B.2.1 Nav420

The Nav420 (Figure B.2) is a solid state data acquisition sensor made by Crossbow, which combines a Global Positioning System (GPS), attitude sensor, and position sensor to measure roll, pitch yaw, surge, sway, and heave. This provides a complete picture of the dynamics for the ship. The data is output though a serial connection at a configurable frequency. This data was then fed into the RMP model simulation to reproduce the ship's dynamics at the time of the trial.

Figure B.2: Nav420 sensor by Crossbow

B.2.2 Motion Capture

Two motion capture systems were used to record the participants' motions during the experiments:

1. Natural Point OptiTrack full body motion capture system with Arena software. This system uses reflective markers and eight cameras positioned around the ship's lab to record body positions.

2. Microsoft Kinect sensors and iPi Recorder/Studio software packages. This system use the Kinects depth camera to determine the positions and orientations of joints in 3D-space.

The primary motion capture system used was the one from Natural Point. The setup consisted of eight high frame-rate cameras (up to twelve can be used) at various positions around the ship's lab and thirty-eight reflective markers attached to a skin-tight, black suit worn by the subject (see Figure 5.2).

Before each experiment, the eight cameras had to be re-calibrated to ensure the Arena software could identify the location in 3D space of each of the markers. This calibration was done by tracking the position of a single marker as it travelled through the field of view of all the cameras. Once that was completed, a square ruler with three directional arrows is placed on the ground in front of the subject to indicate the location and orientation of the ground plane.

Next the subject wore the black suit with the reflective markers positioned to easily identify the body parts. They were required to hold a T-pose while the software ensured it could identify all reflective markers. Once the markers were mapped to body parts the motion capture could commence.

The second motion capture system used was the Kinect from Microsoft. Two versions of the Kinect are available; an XBox 360 version and a Windows PC version. Both types were used in these experiments. Microsoft's motion capture software is free for personal and academic use but it only supports processing data from a single sensor. For this reason, a commercial package called iPi Software was used to combine the sensor data from two Kinects into one 3D skeletal model. This was done to alleviate issues arising from joint occlusion. One camera was placed in-front of the subject and the other behind.

Each Kinect sensor records two streams of data. One is a video stream and the other is a depth stream image. The colours in the depth stream represent the distance from the subject. Depth is determined by emitting and detecting an infra-red signal and comparing the results to a previous image in memory.

The two-sensor Kinect motion capture system can produce results reasonably close to the Natural Point system without the need for a motion capture suit or the lengthy calibration time required for the latter. Two software packages were used to process the Kinect sensor data: iPi Recorder and iPi Studio. The iPi recorder package records and plays back the depth streams while the iPi Studio package maps the motions to a 3D skeletal model.

Before each experimental session it is necessary to re-calibrate each of the Kinect sensors to determine their relative positions and orientations in 3D space. This is done by recording the motion of a flat 2D surface, such as a piece of cardboard, by both cameras concurrently. The iPi Studio software then determines the corners and center of the plane and assumes both sensors are viewing the same object.

B.3 Sea Conditions

The sea trial took place about fifty nautical miles off the coast of Nova Scotia in an area called the Emerald Basin. Four wave buoys were deployed to record significant wave heights during the trial and the ship performed manoeuvres around the buoys. Figure B.3 shows the wave heights recorded by one of the four buoys. The graph shows two significant periods where wave heights had sufficient amplitude to gather meaningful postural stability data. The first few days were used by the researchers to set up and test the data acquisition systems before performing meaningful experiments. The data from the first few days of setup was not used to validate the RMP model for several reasons:

- The data was not collected in a consistent manner as the collection process was still being 'ironed out'.
- The researchers were not used to balancing at sea, so many of the MIIs were not a result of the dynamics of the ship.

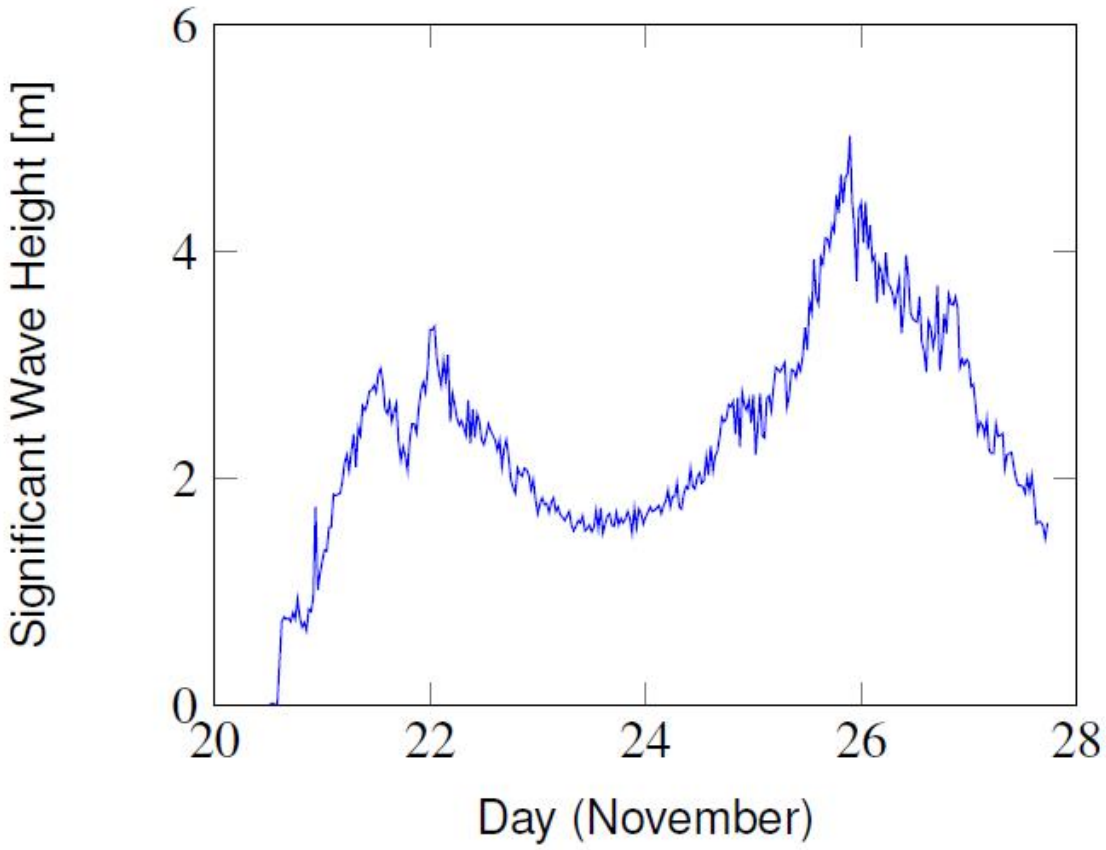

Figure B.3: Significant Wave Heights during the eight day trial.

Appendix C

MII Data

This appendix presents the identified MIIs for each of the ten participants that were used to validate the RMP model. It compares the identified MII times to the times predicted by the RMP model and the times predicted by the IP model. For the stance orientations, the following conventions apply:

- 0° - Participant faces the bow of the ship
- 45° - Participant turns towards the port side 45°
- 90° - Participant faces port side

Times are listed in Greenwich Mean Time (GMT). Some of the subjects encounter no MIIs due to the low sea-state at the time of their trial. The times of identified and predicted MIIs are listed as seconds since the start time.

Participant - Q1

The data collected for participant Q1 on the 24th of November 2012 can be found in Table C.1.

Table C.1: Identified and Predicted MII Times

Start Time	**Stance Orientation**	**Actual Time**	**RMP Time**	**IP Time**
17:32	90.0	None	None	None
17:39	45.0	None	None	None
17:47	0.0	None	None	None
17:57	90.0	87.7	None	None
18:10	45.0	None	None	None
18:17	0.0	None	None	None

Participant - Q2

The data collected for participant Q2 on the 24th of November 2012 can be found in Table C.2.

Table C.2: Identified and Predicted MII Times

Start Time	**Stance Orientation**	**Actual Time**	**RMP Time**	**IP Time**
19:22	90.0	215.0 283.6	54.8	54.8 177.5 211.3 280.6
19:29	45.0	190.8	None	None
19:40	0.0	None	None	None
19:49	90.0	294.8	None	None
19:58	45.0	None	None	138.4 150.0 174.6
20:06	0.0	None	None	None

Participant - Q3

The data collected for participant Q3 on the 25th of November 2012 can be found in Table C.3.

Table C.3: Identified and Predicted MII Times

Start Time	**Stance Orientation**	**Actual Time**	**RMP Time**	**IP Time**
18:52	0.0	None	None	None
19:01	45.0	24.2	24.0	None
		262.7	34.5	
19:08	90.0	29.0	31.9	32.7
		43.2	38.3	38.5
		104.2	51.5	40.6
		127.1	58.4	43.2
		132.3	64.7	65.4
		142.8	72.0	67.8
		170.1	82.8	69.1
		236.1	94.8	106.0
		245.3	105.0	123.4
		247.1	123.0	126.8
		257.9	132.2	288.9
		267.9	139.3	292.0
		282.9	164.9	
		288.1	171.7	
		292.3	212.2	
		296.8	238.7	
			248.6	
			258.8	
			264.9	
19:16	0.0	22.7	None	None
		261.1		
19:24	45.0	22.5	33.6	45.8
		27.2	45.4	47.0
		40.8	54.6	55.2

Continued on next page

Table C.3 – *Continued from previous page*

Start Time	**Stance Orientation**	**Actual Time**	**RMP Time**	**IP Time**
		43.3	64.9	56.4
		56.6	74.1	67.1
		57.5	82.6	75.2
		74.6	88.6	110.8
		75.7	110.3	111.9
		108.4	121.7	122.5
		142.6	128.3	132.1
		143.3	141.3	133.1
		165.3	155.8	134.7
		166.0	163.9	141.7
		184.3	171.5	142.8
		189.7	183.3	157.1
		194.2	192.4	166.1
		200.2	202.6	172.8
		211.5	212.0	193.3
		219.9	220.1	203.3
		243.1	237.6	204.5
		251.4	244.4	284.4
		252.3	251.0	
		256.6	260.2	
		271.2	266.6	
		284.4	275.1	
		292.5	283.0	
		298.4	292.6	
		301.8		
19:30	90.0	30.9	24.9	33.2
		49.7	42.4	47.9
		68.2	47.0	66.6

Continued on next page

Table C.3 – *Continued from previous page*

Start Time	**Stance Orientation**	**Actual Time**	**RMP Time**	**IP Time**
		76.8	55.0	76.1
		77.8	61.5	76.9
		89.5	67.7	77.7
		92.5	74.9	86.9
		118.3	85.8	87.9
		119.6	96.4	88.9
		135.0	107.8	95.0
		135.8	117.1	117.7
		183.3	125.2	118.6
		188.3	133.8	119.5
		194.2	141.0	125.9
		210.8	152.3	127.6
		226.7	161.9	169.6
		241.7	168.7	171.1
		242.9	178.0	178.3
		257.6	189.0	189.7
		279.8	196.9	190.8
		285.0	204.9	196.6
		290.4	212.5	205.2
			223.0	214.9
			231.4	223.5
			237.3	224.4
			247.9	230.6
			259.4	241.3
			269.5	242.4
			277.7	249.0
			288.4	260.3
			295.4	262.6

Continued on next page

Table C.3 – *Continued from previous page*

Start Time	**Stance Orientation**	**Actual Time**	**RMP Time**	**IP Time**
				271.0
				272.4
				278.9
				279.3
				289.8

Participant - Q4

The data collected for participant Q4 on the 25th of November 2012 can be found in Table C.4.

Table C.4: Identified and Predicted MII Times

Start Time	**Stance Orientation**	**Actual Time**	**RMP Time**	**IP Time**
22:14	0.0	None	None	None
22:21	45.0	None	None	None
22:28	90.0	None	None	None
22:38	0.0	None	None	None
22:44	45.0	None	None	None
22:51	90.0	None	None	None

Participant - Q5

The motion capture data for participant Q5 was corrupted and no useful MIIs could be identified for this data set.

Participant - Q6

The data collected for participant Q6 on the 26th of November 2012 can be found in Table C.5.

Table C.5: Identified and Predicted MII Times

Start Time	**Stance Orientation**	**Actual Time**	**RMP Time**	**IP Time**
14:14	0.0	None	None	None
14:21	45.0	57.0 58.1 61.4	57.3	57.0 58.1 61.4
14:28	90.0	14.9 73.4 146.0 246.0 250.0	144.6 244.9 250.8 267.0	245.0 249.7 254.6 261.1 262.9 267.6
14:36	0.0	None	None	None
14:44	45.0	None	None	None
14:52	90.0	49.3	None	None

Participant - Q7

The data collected for participant Q7 on the 27th of November 2012 can be found in Table C.6.

Table C.6: Identified and Predicted MII Times

Start Time	**Stance Orientation**	**Actual Time**	**RMP Time**	**IP Time**
13:28	0.0	None	None	None
13:35	45.0	None	None	None
13:43	90.0	None	None	None
13:49	0.0	None	None	None
13:56	45.0	None	None	None
14:03	90.0	178.0	None	None

Participant - D1

The ship motion data for participant D1 was corrupted so no MIIs could be predicted for this data set.

Participant - D2

The data collected for participant D2 on the 25th of November 2012 can be found in Table C.7.

Table C.7: Identified and Predicted MII Times

Start Time	**Stance Orientation**	**Actual Time**	**RMP Time**	**IP Time**
12:59	90.0	84.4	26.3	16.2
		141.1	45.3	25.8
			87.9	105.3
			95.7	114.6
			104.1	144.9
			113.2	246.5
			144.8	

Continued on next page

Table C.7 – *Continued from previous page*

Start Time	**Stance Orientation**	**Actual Time**	**RMP Time**	**IP Time**
			246.3 258.0	
13:08	45.0	None	None	174.1
13:16	0.0	None	None	None
13:23	90.0	297.4	290.9 297.9	117.8 129.2 131.0 297.0
13:31	45.0	289.5	82.5	284.5
13:40	0.0	None	None	None
13:46	90.0	83.6	30.7 80.1 97.4 103.1 141.5 150.1 165.3 200.7 236.7 245.3 292.5	None

Participant - D3

The data collected for participant D3 on the 25th of November 2012 can be found in Table C.8.

Table C.8: Identified and Predicted MII Times

Start Time	**Stance Orientation**	**Actual Time**	**RMP Time**	**IP Time**
14:29	0.0	None	None	None
14:36	45.0	20.0 178.0 195.1 262.2	16.7	None
14:44	90.0	173.2	None	167.0 211.9 223.2 232.6 268.1 288.8 299.9
14:50	0.0	None	None	None
14:57	45.0	14.9 19.2	None	None
15:04	90.0	83.8 95.1 96.7 102.8 136.2 162.8 164.8 166.2 195.2 294.7	94.0 99.9 134.2 140.2 161.3 167.1 173.5 232.0 262.1 292.6	98.8 121.4 134.6 166.8 232.5 253.1 262.4 292.3 297.1
15:11	90.0	18.5 83.4	76.0 157.4	18.5 83.4

Continued on next page

Table C.8 – *Continued from previous page*

Start Time	**Stance Orientation**	**Actual Time**	**RMP Time**	**IP Time**
		161.0	177.9	161.0
		164.7	232.6	164.7
		181.4		181.4
		232.3		232.1

Bibliography

[1] A.E. Baitis, T.R. Applebee, and T.M. McNamara. Human Factors Considerations Applied to Operations of the FFG-8 and Lamps MK III. *Naval Engineers Journal*, 97(4):191–199, 1984.

[2] A.E. Baitis, F.D. Holcomb, S.L. Conwell, P. Crossland, J.H. Patton, and R. Strong. Motion Induced Interruption (MII) and Motion Induced Fatigue (MIF) experiments at the Naval Biodynamics Laboratory. Technical Report CRDKNSWE-HD-1423-01, Carderock Division, Naval Surface Warfare Center, 1995.

[3] F. Benvenuti. Physiology of Human Balance. *Advances in Neurology*, 87:41–51, 2001.

[4] K. Bothner and J. Jensen. How Do Non-Muscular Torques Contribute to the Kinetics of Postural Recovery Following a Support Surface Translation. *Journal of Biomechanics*, 34(2):245–250, 2001.

[5] C.K. Chow and D.H. Jacobson. Further Studies of Human Locomotion Postural Stability and Control. *Mathematical Biosciences*, 15:93–108, 1972.

[6] J.J. Craig. *Introduction to Robotics: Mechanics and Control*. Addison-Wesley, Reading, MA, 1989.

[7] P. Crossland. Using the Large Motion Simulator (LMS) at DRA Bedford to Investigate the Effects of Ship Motions on Motion Induced Interruptions. Technical Report DRA/SS/SSHE/CR96008, Defence Research Agency, 1996.

[8] P. Crossland. Validating a Model for Predicting Motion Induced Interruptions to Task Performance Using Simulated Motions From the FFG-8 and Type 23 Frigate. Technical Report DERA/SS/HE/CR971017, Defence Evaluation and Research Agency, 1997.

[9] P. Crossland, M.J. Evans, D. Grist, M. Lowten, H. Jones, and R.S. Bridger. Motion-induced interruptions aboard ship: Model development and application to ship design. *Occupational Ergonomics*, 7(3):183–199, 2007.

[10] P. Crossland and K. Rich. Validating a Model of the Effects of Ship Motion on Postural Stability. *International Conference of Environmental Ergonomics*, pages 385–388, 1998.

[11] C.A. Duncan, S.N. MacKinnon, and W.J. Albert. Changes in thoracolumbar kinematics and centre of pressure when performing stationary tasks in moving environments. Technical report, Memorial University of Newfoundland, 2009.

[12] C.A. Duncan, S.N. MacKinnon, W.J. Alberta, D.M. Antle, and J. Matthews. Effect of simulated vessel motions on thoracolumbar and centre of pressure kinematics. *Occupational Ergonomics*, 7:265–274, 2007.

[13] R. Featherstone. The calculation of robot dynamics using articulated-body inertias. *The International Journal of Robotics Research*, 2(1):13–30, 1983.

[14] R. Featherstone. *Robot Dynamics Algorithms*. Kluwer Academic Publishers, Norwell, MA, 1987.

[15] G.E. Gehl. *Assessing Motion Induced Interruptions Using A Motion Platform*. Master of Science in Human Systems Integration, Naval Post Graduate School, Monterey California, September 2013.

[16] R. Graham. Motion Induced Interruptions as Ship Operability Criteria. *Naval Engineers Journal*, 102(2):65–71, 1990.

[17] R. Graham, A. Baitis, and W. Meyers. On the development of seakeeping criteria. *Naval Engineers Journal*, 104(3):259–275, May 1992.

[18] F. Gubina, H. Hemami, and R.B. McGhee. On the Dynamic Stability of Biped Locomotion. *IEEE Transactions on Biomedical Engineering*, 21(2):102–108, 1974.

[19] C.J. Hasson, R.E. Van Emmerik, and G.E Caldwell. Predicting dynamic postural instability using center of mass time-to-contact information. *Journal of Biomechanics*, 41(10):2121–2129, 2008.

[20] H. Hemami. The Inverted Pendulum and Biped Stability. *Mathematical Biosciences*, 34(2):95–110, 1977.

[21] H. Hemami, K. Barin, and Y. Pai. Quantitative Analysis of the Ankle Strategy Under Translational Platform Disturbances. *IEEE Transactions on Neural Systems and Rehabilitation Engineering*, 14(4):470–480, 2006.

[22] H. Hemami and C.L.J. Golliday. Postural Stability of the Two-Degree-Of-Freedom Biped by General Linear Feedback. *IEEE Transations on Automatic Control*, 21:74–79, 1976.

[23] H. Hemami, M.J. Hines, R.E. Goddard, and B. Friedman. Biped Sway in the Frontal Plane with Locked Knees. *IEEE Transactions on Systems, Man and Cybernetics*, SMC–12(4):577–582, 1982.

[24] H. Hemami and V.C. Jaswa. On a Three-Link Model of the Dynamics of Standing Up and Sitting Down. *IEEE Transactions on Systems, Man and Cybernetics*, SMC–8:120–135, 1978.

[25] A.L. Hof, M.G.J. Gazendam, and W.E. Sinke. The condition for dynamic stability. *Journal of Biodynamics*, 38:1–8, 2005.

[26] L. Humphrey, H. Hemami, K. Barin, and A. Krishnamurthy. Simulated Responses to Support Surface Disturbances in Humanoid Biped Model With a Vestibular-Like Apparatus. *IEEE Transactions on Systems, Man and Cybernetics*, 40(1):109–119, 2010.

[27] K. Iqbal, H. Hemami, and S. Simon. Stability and Control of a Frontal Four-Link Biped System. *IEEE Transations on Biomedical Engineering*, 40(10):1007–1018, 1993.

[28] S. Kiemel. Balance maintenance of a humanoid robot using the hip-ankle strategy. Master's thesis, Delft University of Technology, 2012.

[29] S.H. Koozekanani, C.W. Stockwell, R.B. McGhee, and F. Firoozmand. On the Role of Dynamic Models in Quantitative Posturography. *IEEE Transactions on Biomedical Engineering*, BME–27(10):605–609, 1980.

[30] R.G. Langlois. Development of a Spatial Inverted Pendulum Shipboard Postural Stability Model. Technical report, Carleton University, 2010.

[31] R.G. Langlois, N. Bourgeois, M.J. Leveille, H. Morris, and A.M. Wice. Human Postural Stability Models. Technical report, Carleton University, February 2013.

[32] R.G. Langlois, S.N. Mackinnon, and C.A. Duncan. Modelling Sea Trial Motion Induced Interruption Data Using an Inverted Pendulum Articulated Postural Stability Model. *International Journal of Maritime Engineering*, 151:1–10, 2009.

[33] S. Lee and A. Goswami. Reaction mass pendulum (RMP): An explicit model for centroidal angular momentum of humanoid robots. *Robotics and Automation*, pages 4667–4672, 2007.

[34] S. Lee and A. Goswami. The reaction mass pendulum (RMP) model for humanoid robot gait and balance control. *Humanoid Robots*, 71:167–186, 2009.

[35] B.E. Maki and W.E. McIlroy. The Role of Limb Movements in Maintaining Upright Stance: The Change-in-Support Strategy. *Physical Therapy*, 77(5):488–507, 1997.

[36] P. Matsangas and M.E. McCauley. Motion-Induced Interruptions and Postural Equilibrium in Linear Lateral Accelerations. Technical report, Monterey, California. Naval Postgraduate School, 2013.

[37] J. Matthews, S. Mackinnon, W. Albert, M. Holmes, and A. Patterson. Effects of Moving Environments on the Physical Demands of Heavy Materials Handling Operators. *International Journal of Industrial Ergonomics*, 37(1):43–50, 2007.

[38] W.E. McIlroy and B.E. Maki. Task Constraints on Foot Movement and the Incidence of Compensatory Stepping Following Pertubation of Upright Stance. *Brain Research*, 616:30–38, 1993.

[39] J. Mckee. *Simulating the Effects of Ship Motion on Postural Stability Using Articulated Dynamic Models*. Phd thesis, Carleton University, 2004.

[40] L.M. Nashner. *Sensory Feedback in Human Posture Control*. Phd thesis, Massachusetts Institute of Technology, 1970.

[41] L.M. Nashner. Adaptation of Human Movement to Altered Environments. *Trends in Neurosciences*, 5:358–361, 1982.

[42] J.L. Patton, Y.C. Pai, and W.A. Lee. A Simple Model of the Feasible Limits to Postural Stability. In *Engineering in Medicine and Biology Society*, volume 4, pages 1679–1682, 1997.

[43] J.L. Patton, Y.C. Pai, and W.A. Lee. Evaluation of a Model that Determines the Stability Limits of Dynamic Balance. *Gait and Posture*, 9:38–49, 1999.

[44] H.P.M. Peeters, H.B. Caberg, and J.M.F Mol. Evaluation of Biomechanical Models in Posturography. *Medical and Biological Engineering and Computing*, 23(5):469–473, 1985.

[45] J. Pratt, J. Carff, S. Drakunov, and A. Goswami. Capture point: A step toward humanoid push recovery. *Humanoid Robots*, 6:200–207, 2006.

[46] J. Pratt, C.M. Chew, A. Torres, P. Dilworth, and G. Pratt. Virtual model control: An intuitive approach for bipedal locomotion. *The International Journal of Robotics Research*, 20(2):129–143, 2001.

[47] J. Pratt, T. Koolen, T. De Boer, J. Rebula, S. Cotton, J. Carff, and P. Neuhaus. Capturability-based analysis and control of legged locomotion, Part 2: Application to M2V2, a lower-body humanoid. *The International Journal of Robotics Research*, 31(10):1117–1133, 2012.

[48] J. Pratt and G. Pratt. Intuitive control of a planar bipedal walking robot. *Robotics and Automation*, 3:2014–2021, May 1998.

[49] R.E. Roberson and R. Schwertassek. *Dynamics of Multibody Systems*, volume 18. Berlin: Springer-Verlag, 1988.

[50] J.E. Scrivens, L.H. Ting, and S.P. DeWeerth. Effects of Stance Width on Control Gain in Standing Balance. *Engineering in Medicine and Biology Society*, EMBS 2006:4055–4057, 2006.

[51] C.W. Stockwell, S.H. Koozekanai, and K. Barin. A Physical Model of Human Postural Dynamics. *Annals of the New York Academy of Sciences*, 374:722–730, 1981.

[52] T.A. Stoffregen, S. Villard, F. Chen, and Y. Yu. Standing Posture on Land and at Sea. *Ecological Psychology*, 23(1):19–36, 2011.

[53] H. William. *Numerical recipes in C++: the art of scientific computing*. Cambridge University Press, 2nd edition, 2002.

[54] D.A. Winter, A.E. Patla, P. Francois, M. Ishac, and K. Gielo-Perczak. Stiffness Control of Balance in Quiet Standing. *Journal of Neurophysiology*, 5:1211–1221, 1998.

[55] Q. Wu and R. Swain. On Lyapunovs Stability Control of Two-Link Base Excited Inverted Pendulums with Applications to Human Locomotion. In *IEEE International Conference on Systems, Man, and Cybernetics*, volume 5, pages 3330–3335, 2000.

[56] Q. Wu, A.B. Thornton-Trump, and N. Sepehri. Lyapunov Stability Control of Inverted Pendulums with General Base Point Motion. *International Journal of Non-Linear Mechanics*, 33(5):801–818, 1998.

[57] J.S. Yuan. Closed-loop manipulator control using quaternion feedback. *Robotics and Automation*, 4(4):434–440, 1988.